LETTER

doi:10.1038/nature19364

Ionic immune suppression within the tumour microenvironment limits T cell effector function

Robert Eil[1]*†, Suman K. Vodnala[1]*, David Clever[1], Christopher A. Klebanoff[1,2], Madhusudhanan Sukumar[1], Jenny H. Pan[1], Douglas C. Palmer[1], Alena Gros[1]†, Tori N. Yamamoto[1], Shashank J. Patel[1], Geoffrey C. Guittard[1], Zhiya Yu[1], Valentina Carbonaro[3], Klaus Okkenhaug[3], David S. Schrump[1], W. Marston Linehan[1], Rahul Roychoudhuri[3] & Nicholas P. Restifo[1]

Tumours progress despite being infiltrated by tumour-specific effector T cells[1]. Tumours contain areas of cellular necrosis, which are associated with poor survival in a variety of cancers[2]. Here, we show that necrosis releases intracellular potassium ions into the extracellular fluid of mouse and human tumours, causing profound suppression of T cell effector function. Elevation of the extracellular potassium concentration ($[K^+]_e$) impairs T cell receptor (TCR)-driven Akt–mTOR phosphorylation and effector programmes. Potassium-mediated suppression of Akt–mTOR signalling and T cell function is dependent upon the activity of the serine/threonine phosphatase PP2A[3,4]. Although the suppressive effect mediated by elevated $[K^+]_e$ is independent of changes in plasma membrane potential (V_m), it requires an increase in intracellular potassium ($[K^+]_i$). Accordingly, augmenting potassium efflux in tumour-specific T cells by overexpressing the potassium channel $K_v1.3$ lowers $[K^+]_i$ and improves effector functions *in vitro* and *in vivo* and enhances tumour clearance and survival in melanoma-bearing mice. These results uncover an ionic checkpoint that blocks T cell function in tumours and identify potential new strategies for cancer immunotherapy.

The tumour microenvironment is characterized in part by rapidly dividing cancer cells competing for limited local resources[5,6]. These factors cause dense areas of cellular apoptosis and necrosis[2]. Tumour necrosis is frequently associated with a poor prognosis[2]. Additionally, necrosis alters the extracellular milieu in association with the release of intracellular ions[7,8]. Although tumour-specific T cells harbour reactivity against tumour antigens[9], their function is often suppressed within tumours[1]. Whether local necrosis or consequent ionic imbalances contribute to T cell dysfunction within tumours is unknown.

Multiple lines of investigation have demonstrated that intact ion transport is required for T cell function. Mutations that affect of store-operated Ca^{2+}entry result in severe combined immunodeficiency (SCID) in humans[10]. Moreover, voltage-gated Ca^{2+} channels are essential for T cell function and survival[11] and mutations in the Mg^{2+} channel MAGT1 lead to human T cell immunodeficiency[12]. Finally, overabundance of Na^+ and Cl^- promotes T cell pathogenicity and autoimmunity via the kinase SGK-1 (ref. 13). Despite ions playing a key role in T cell function, their extracellular concentrations and functional relevance within tumours are poorly understood.

We hypothesized that tumour cell death leads to a local ionic imbalance within the tumour microenvironment. To isolate native undiluted extracellular fluid within tumours, hereafter termed tumour interstitial fluid (TIF), we used a centrifugation method[14] as previously described[6,15]. This enabled us to compare the concentrations of five principal ions in TIF from mouse B16 melanomas or human tumours with those in serum. $[K^+]$ was higher in TIF than in serum in both mouse and human tumours (Fig. 1a, b and Extended Data Fig. 1a) but not in extracellular fluid isolated from healthy tissues (Extended Data Fig. 1b). We also observed a correlation between TIF $[K^+]$ and the density of dying cells within mouse B16 tumours (Fig. 1c). Additionally, experimental induction of cell death or apoptosis in tumour-derived cell lines increased extracellular potassium concentration ($[K^+]_e$) (Fig. 1d and Extended Data Fig. 1c, d). Thus, we conclude that the extracellular space within tumours contains elevated $[K^+]_e$, which is associated with local cellular apoptosis and necrosis.

We next investigated whether elevated $[K^+]_e$ affects T cell function. We found that isotonic elevations in $[K^+]_e$ produced dose-dependent suppression of TCR-induced cytokine production (Fig. 1e, f). Elevated $[K^+]_e$ acted independent of tonicity, with other monovalent and divalent ions or inert osmolytes failing to induce similar suppression (Fig. 1f, g and Extended Data Fig. 1e–h). Elevated $[K^+]_e$ acutely suppressed T cell activation across a range of signal strengths (Extended Data Fig. 1i), in the presence or absence of co-stimulation (Extended Data Fig. 1j), in a non-redundant fashion with tumour-associated co-inhibitory signals (Fig. 1h, i and Extended Data Fig. 2a, b), in $CD4^+$ T_H1 and T_H17 effector subtypes (Extended Data Fig. 2c, d). However, it had no effect on cellular viability (Extended Data Fig. 2e). We next isolated endogenous human neoantigen-specific tumour infiltrating lymphocytes (TILs), which have been identified as likely mediators of immunotherapy-induced tumour clearance[9,16], and found that interferon-γ (IFNγ) production by these cells in response to their cognate neoepitope was attenuated by elevated $[K^+]_e$ (Fig. 1j and Extended Data Fig. 2f, g). Elevated $[K^+]_e$ also led to suppression of target-specific IFNγ production by T cells genetically engineered to carry a cancer-germline-antigen-specific TCR[17](Extended Data Fig. 2h). Thus, our data suggest that elevated $[K^+]_e$ acutely limits the function of mouse and human T cells.

To understand the basis of this suppression of effector function, we investigated the effect of elevated $[K^+]_e$ on the molecular events driven by TCR engagement. To this end, we briefly activated fluorescence-activated cell sorting (FACS)-purified mouse $CD8^+$ T cells in the presence or absence of elevated $[K^+]$ and found that elevated $[K^+]_e$ reduced the expression of transcripts induced by TCR stimulation (Fig. 2a, b). Furthermore, gene-set enrichment analysis indicated that elevated $[K^+]_e$ suppressed genes induced by TCR signalling, NF-κB activation, escape from anergy, the adaptive immune response and cytokine pathways (Supplementary Information 1). Collectively, these data suggest that intratumoural cell death produces elevated $[K^+]_e$ concentrations that suppress TCR-driven effector programmes.

As elevated $[K^+]_e$ acutely suppressed TCR-driven transcriptional events, we investigated whether $[K^+]_e$ could affect TCR-induced signal transduction pathways. Given the role of $[K^+]_e$ in regulating plasma membrane potential[18,19], we initially hypothesized that K^+ suppressed

[1]National Cancer Institute, National Institutes of Health (NIH), Bethesda, Maryland 20892, USA. [2]Center for Cell Engineering and Department of Medicine, Memorial Sloan Kettering Cancer Center, New York, New York 10065, USA. [3]Laboratory of Lymphocyte Signalling and Development, The Babraham Institute, Cambridge CB22 3AT, UK. †Present addresses: Department of Surgery, Oregon Health and Sciences University, Portland, Oregon 97239, SA (R.E.); Vall d'Hebron Institute of Oncology VHIO, Vall d'Hebron University Hospital, c/Natzaret, 115-117, Barcelona 08035, Spain (A.G.). *These authors contributed equally to this work.

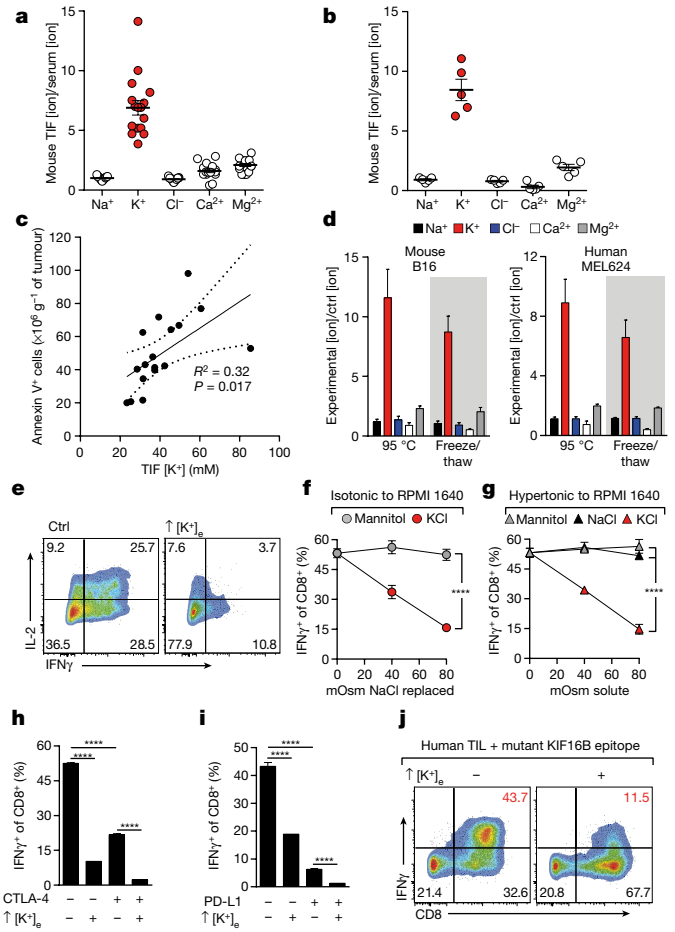

Figure 1 | Elevated $[K^+]$ within TIF silences the TCR-induced anti-tumour function of mouse and human T cells. a, **b**, Ratiometric representation of TIF to serum values for the indicated ions from mouse (**a**) and human (**b**) tumour tissue. **c**, Linear regression and 95% CI best fit line representing the relationship between TIF $[K^+]$ and annexin V^+ cells per g of tumour. Significance calculated by Pearson's correlation coefficient. **d**, Extracellular concentration of electrolytes following induction of cell death as indicated for mouse (left) and human (right) tumour cell lines. **e**–**i** Anti-CD3 and -CD28 (anti-CD3/CD28)-based activation of $CD8^+$ mouse T cells in the indicated conditions with representative flow cytometry (**e**), additional $[K^+]_e$ equal to 40 mM unless otherwise indicated and quantification (**f**–**i**). **j**, Human TILs stimulated in the indicated conditions with mutated neo-antigen peptide-pulsed target cells (autologous B cells), additional $[K^+]_e = 50$ mM. Centre values and error bars represent mean ± s.e.m. $*P < 0.05$; $**P < 0.01$; $***P < 0.001$; $****P < 0.0001$ between selected relevant comparisons, **f**, **g** two-way ANOVA; **h**, **i**, two-tailed Student's *t*-tests. **a**, **c**, $n = 18$ biological replicates; **b**, $n = 5$ biological replicates; **d**, $n = 4$ culture replicates; **e**–**i**, $n = 3$ culture replicates per condition; **j**, $n = 3$ culture replicates; representative of three (**e**–**g**) or two (**h**–**j**) independent experiments.

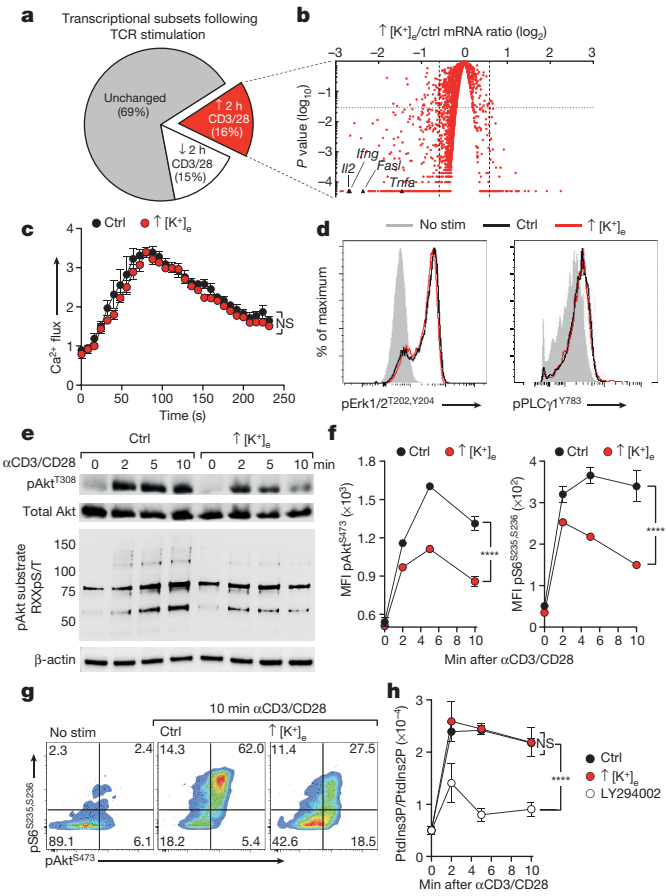

Figure 2 | $[K^+]_e$ inhibits TCR-induced transcripts and function by suppressing Akt–mTOR phosphorylation. a, Pie chart representing proportional subpopulations of all transcripts following 2 h re-stimulation of purified $CD8^+$ T cells with anti-CD3/CD28. **b**, Volcano plot of TCR-induced genes briefly re-stimulated with anti-CD3/CD28 in the indicated conditions. **c**, TCR cross-linking induced calcium flux of $CD8^+$ cells as measured by the quotient of Fluo3 and FuraRed fluorescence in the indicated conditions. **d**, Representative phosphoflow cytometry plots following TCR cross-linking in the indicated conditions. **e**, Immunoblot analysis of the indicated phospho-residues in $CD8^+$ T cells following TCR cross-linking. **f**, Quantitative phosphoflow analysis of cells activated as in **c** and **d** with representative flow cytometry in **g**. **h**, Quantification of the indicated phosphatidylinositol species in $CD8^+$ T cells activated via TCR cross-linking in the indicated conditions. Centre values and error bars represent mean ± s.e.m. $*P < 0.05$; $**P < 0.01$; $***P < 0.001$; $****P < 0.0001$ between selected relevant comparisons, two-way ANOVA. **c**–**h**, Where noted additional $[K^+]_e = 40$ mM. **a**–**c**, $n = 3$ biological replicates; **d**, **f**, $n = 3$ technical replicates per data point; **h**, $n = 3$ experimental replicates with pooled analysis displayed; **d**–**g**, representative of at least three independent experiments.

TCR activation by inducing cellular membrane depolarization (increased V_m) with subsequent dissipation of the electromotive force driving Ca^{2+} entry. However, we could not detect any changes in TCR-induced Ca^{2+} flux in the presence of isotonic elevations in $[K^+]_e$ (40 mM) (Fig. 2c and Extended Data Fig. 3a). Additionally, elevated $[K^+]_e$ did not affect the phosphorylation of Zap70, Erk1/2 or PLCγ1, or global tyrosine phosphorylation, following TCR ligation (Fig. 2d and Extended Data Fig. 3b, c). However, elevated $[K^+]_e$ did reduce TCR-induced phosphorylation of Akt and serine/threonine residues targeted by Akt (Fig. 2e–g and Extended Data Fig. 3d), including mTOR and the ribosomal protein S6 (Fig. 2f, g and Extended Data Fig. 3d). Suppression of Akt–mTOR signalling by elevated $[K^+]_e$ was noticeable at later time points (Extended Data Fig. 3e), was not replicated by other osmolytes (Extended Data Fig. 4a) and was apparent in conditions of hypertonic hyperkalaemia (Extended Data Fig. 4b). Consistent with a role in limiting Akt–mTOR activity[20], elevated $[K^+]_e$ inhibited TCR-induced nutrient consumption (Extended Data Fig. 4c, d) and $CD4^+$ polarization to effector lineages (Extended Data Fig. 4e, f) and promoted the induction of $Foxp3^+$ $CD4^+$ T cells (Extended Data Fig. 4g). We therefore conclude that elevated $[K^+]_e$ limits TCR-driven effector function via suppression of the Akt–mTOR pathway.

We next aimed to determine how elevated $[K^+]_e$ suppresses TCR-induced Akt–mTOR phosphorylation. First, we hypothesized that elevated $[K^+]_e$ inhibits PI3K activity. However, elevated $[K^+]_e$ had no effect on TCR-induced phosphatidylinositol-3-phosphate (PtdIns3P) accumulation (Fig. 2h), indicating that K^+-mediated suppression of Akt signalling was downstream of PI3K activation. Regulation of Akt activity downstream of PI3K is carried out, in part, by serine/threonine

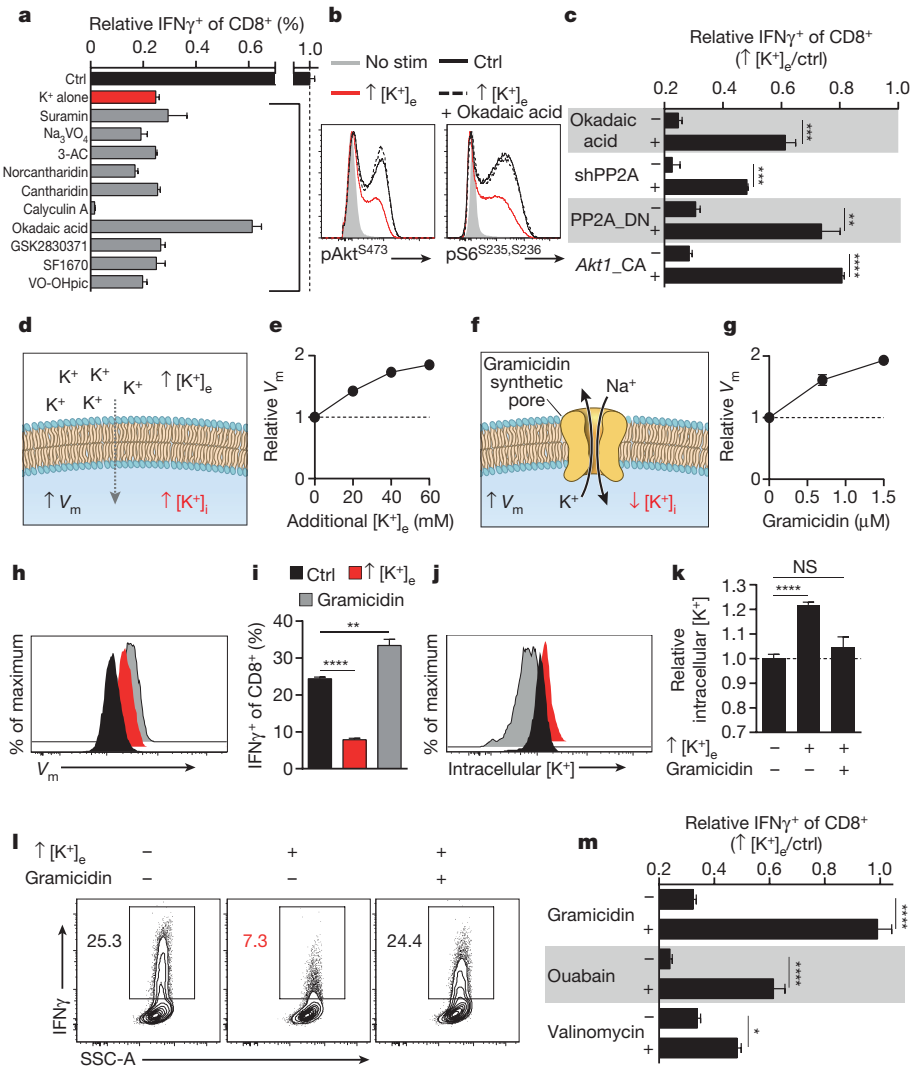

Figure 3 | $[K^+]_e$-mediated T cell suppression requires intact PP2A activity and is associated with elevations in $[K^+]_i$. **a**, Selected phosphatase inhibitors from a pharmacologic screen for IFNγ production of $CD8^+$ T cells in the presence of elevated $[K^+]_e$, depicted as the ratio of IFNγ expression in untreated (ctrl)/elevated $[K^+]_e$ conditions in the presence of indicated phosphatase inhibitors. **b**, $CD8^+$ T cell phosphorylation of $pAkt^{S473}$ and $pS6^{S235,S236}$ 10 min after TCR cross-linking in the indicated conditions. **c**, Compiled analysis of IFNγ production by retrovirally transduced $CD8^+$ Thy1.1$^+$ T cells following TCR stimulation in the indicated conditions. **d**, Pictorial representation of the resultant intracellular changes in V_m and $[K^+]_i$ in the presence of elevated $[K^+]_e$. **e**, Relative cytoplasmic V_m of $CD8^+$ T cells in the indicated conditions represented as relative fluorescence of the voltage-sensitive fluorescent indicator $DiSBAC_4(3)$. **f**, Pictorial representation of the resultant intracellular changes in V_m and $[K^+]_i$ in the presence of gramicidin. **g**, Relative cytoplasmic V_m of $CD8^+$ T cells in the indicated conditions assayed as in **e** with representative flow cytometry in **h**. **i**, IFNγ production by $CD8^+$ T cells following TCR-induced stimulation in the indicated conditions. **j**, Representative flow cytometry representing $[K^+]_i$ of $CD8^+$ T cells as relative fluorescence of the potassium-sensitive dye Asante-Green 4. **k**, Relative $[K^+]_i$ of $CD8^+$ T cells in the indicated conditions assayed as relative fluorescence of Asante-Green 4. **l**, Representative flow cytometry of cytokine expression by $CD8^+$ T cells following TCR stimulation in the indicated conditions with compiled quantification in **m**. Centre values and error bars represent mean ± s.e.m. $*P<0.05$; $**P<0.01$; $***P<0.001$; $****P<0.0001$ between selected relevant comparisons, two-tailed Student's *t*-tests (**a**–**m**). Where noted additional $[K^+]_e = 40$ mM. **a**, **c**, **i**, **l**, **m**, $n =$ at least three culture replicates per data point; **e**, **g**, **h**, **j**, **k**, $n = 3$ technical replicates per data point; representative of at least two (**a**, **b**, **c**, **m**) or three or more (**e**, **g**, **i**, **h**, **l**, **k**) independent experiments.

phosphatases. To interrogate cytokine production in the presence of elevated $[K^+]_e$, we used a pharmacologic screening approach to determine whether selected compounds, including inhibitors of cellular phosphatases, might restore effector function in the presence of elevated $[K^+]_e$ (Fig. 3a). Notably, okadaic acid, an inhibitor of the serine/threonine phosphatase PP2A[21], significantly restored T cell function in the presence of elevated $[K^+]_e$.

Moreover, okadaic acid reversed the hypophosphorylation of Akt and S6 caused by elevated $[K^+]_e$ (Fig. 3b and Extended Data Fig. 5a) in addition to restoring effector function (Fig. 3c and Extended Data Fig. 5b). Similarly, genetic disruption of PP2A function by overexpression of a dominant-negative isoform (PP2A_DN) or by short-hairpin-mediated RNA interference against the PP2A subunit *Ppp2r2d* similarly rescued effector function in the presence of elevated $[K^+]_e$ (Fig. 3c and Extended Data. Fig. 5c, d). Consistent with the mechanistic involvement of Akt–mTOR hypophosphorylation in the suppression of effector function mediated by elevated $[K^+]_e$, we found that T cells expressing a constitutively active form of Akt (*Akt1*_CA) exhibited resistance to the inhibitory effects of high $[K^+]_e$ (Fig. 3c and Extended Data Fig. 5e). Thus, we conclude that elevated $[K^+]_e$ drives hypophosphorylation of the Akt–mTOR pathway in a PP2A-dependent manner.

We next aimed to identify the intracellular changes responsible for decreased Akt–mTOR phosphorylation and cytokine production in the presence of elevated $[K^+]_e$. As K^+ is the principal determinant of

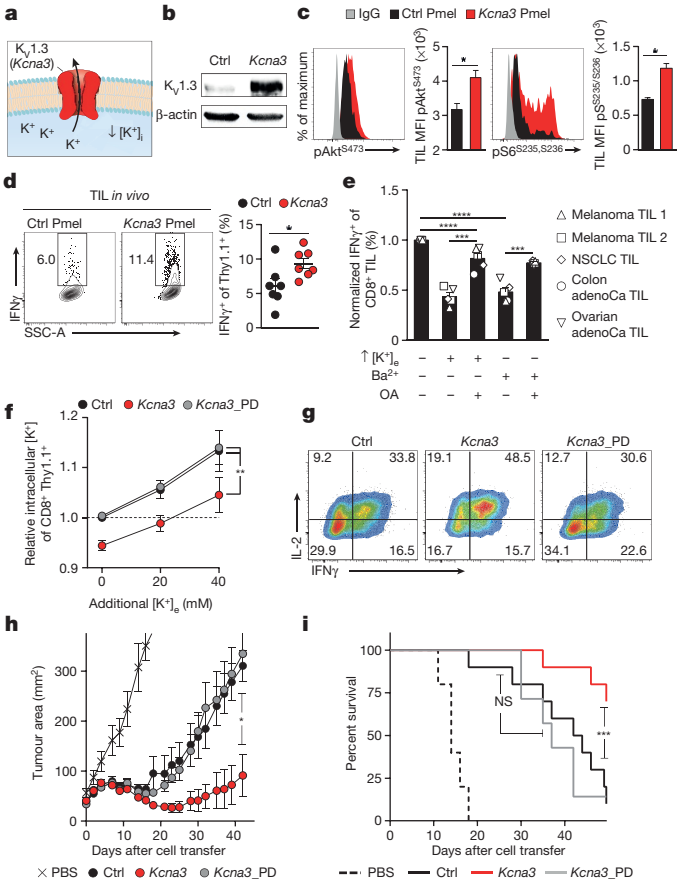

Figure 4 | *Kcna3* overexpression lowers $[K^+]_i$, enhances Akt–mTOR signalling and augments anti-tumour effector function to improve tumour clearance and host survival. a, Pictorial representation of the potassium channel $K_v1.3$ (*Kcna3*). **b**, Representative immunoblot analysis of $K_v1.3$ protein abundance in $CD8^+$ Pmel-1 cells following retroviral transduction with Ctrl (Empty-Thy1.1) or *Kcna3*-Thy1.1 constructs. **c**, **d**, $Thy1.1^+$ Pmel-1 $CD45.1^+CD8^+$ TIL 6–8 days following transfer into B16 melanoma-bearing mice were analysed for indicated phospho-residues (**c**) or *in vivo* IFNγ production 6 h after injection with Brefeldin A (**d**). **e**, Relative cytokine expression of human TILs originating from the indicated histology following TCR stimulation in the indicated conditions. **f**, **g**, Analysis of $[K^+]_i$ (**f**) and representative flow cytometry for the expression of the indicated cytokines (**g**) of $CD8^+$ $Thy1.1^+$ T cells following transduction with retrovirus expressing Ctrl, *Kcna3* or *Kcna3_PD* $Thy1.1^+$ constructs. **h**, **i**, Rates of tumour growth (**h**) and host survival (**i**) represented over time following receipt of Pmel-1 $CD8^+$ T cells transduced as in **f**, **g**. two-tailed Student's *t*-tests (**c**–**e**), two-way ANOVA (**f**), Wilcox rank-sum analysis (**h**), and log-rank of Kaplan–Meier survival estimates (**i**). Centre values and error bars represent mean ± s.e.m. $*P<0.05$; $**P<0.01$; $***P<0.001$; $****P<0.0001$ between selected relevant comparisons, additional $[K^+]_e = 50$ mM in **e**. **c**, $n=5$ mice per group; **d**, $n=7$ mice per group; **e**, each symbol represents the mean of $n=3$ culture replicates per patient per data point; **f**, $n=3$ technical replicates per data point; **h**, **i**, $n=$ at least ten mice per group; representative of three (**b**) or two (**c**–**i**) independent experiments.

resting V_m (refs 18, 19), we first investigated whether increased V_m in the presence of elevated $[K^+]_e$ provided the source of T cell suppression (Fig. 3d, e). To this end we tested whether modulation of V_m by other means in the presence of low $[K^+]_e$ would result in analogous suppression of T cell function. We treated cells with the ionophore gramicidin, which increases V_m by forming pores in the plasma membrane permeable to both Na^+ and K^+ (Fig. 3f–h). However, as gramicidin, unlike elevated $[K^+]_e$, increased IFNγ production (Fig. 3i), we reasoned that suppression of T cell function by high $[K^+]_e$ is independent of the effect of high $[K^+]_e$ on V_m and rather depends upon $[K^+]_i$. Consistent with this hypothesis, elevated $[K^+]_e$ raised $[K^+]_i$ while gramicidin depleted $[K^+]_i$ and reversed the suppression of T cell function induced by high $[K^+]_e$ (Fig. 3j–m and Extended Data Fig. 6a–c). Additionally, other pharmacologic interventions that deplete intracellular K^+, such as treatment with the ionophore valinomycin or inhibition of the Na^+,K^+–ATPase by ouabain, led to the rescue of T cell function in the presence of elevated $[K^+]_e$ (Fig. 3m and Extended Data Fig. 6d–k). Consistent with results from other cell types, we quantified the baseline $[K^+]_i$ of T cells as 133.8 ± 3.3 mM. Additions of 20 or 40 mM $[K^+]_e$ increased $[K^+]_i$ to 143 ± 4.5 mM or 153.2 ± 4.4 mM, respectively (Extended Data Fig. 7a, b). T cells chronically exposed to elevated $[K^+]_e$ responded to subsequent $[K^+]_e$ changes similarly to those cultured in control conditions (Extended Data Fig. 7c–f), whereas brief exposure to ouabain partially reversed elevations in $[K^+]_i$ and T cell suppression in the presence of high $[K^+]_e$ (Fig. 3m and Extended Data Fig. 6h–k). Together, these data suggest that elevated $[K^+]_i$ in the presence of elevated extracellular K^+ concentrations may result from a combination of augmented Na^+,K^+-ATPase function and a relative decrease in K^+ flow per channel as the dynamically equilibrated chemical gradient between the intracellular and extracellular space, and the absolute reversal potential for K^+, is attenuated.

Collectively, our findings suggested that enhancing T cell K^+ efflux might increase T cell anti-tumour function. Previous investigations of T-cell-intrinsic K^+ transport, focusing on the voltage-gated potassium channel $K_v1.3$ encoded by *Kcna3* and the calcium-gated potassium channel $K_{Ca}3.1$ (*Kcnn4*), have described dynamic regulation of K^+ transport in association with T cell activation and differentiation state[22,23]. Brief re-stimulation of mouse $CD8^+$ effector cells *in vitro* (Fig. 2b) revealed acute upregulation of *Kcna3* mRNA in addition to dynamic expression of transcripts encoding potassium channels, pumps, and regulatory subunits (Supplementary Information 2). Because *Kcna3* can be induced by TCR activation and has a role in T cell function[24], we hypothesized that enforced expression of *Kcna3* might increase K^+ efflux and thereby increase intratumoural T cell effector function. We found that overexpression of *Kcna3* in mouse T cells (Fig. 4a, b) resulted in lower T cell $[K^+]_i$ (Extended Data Fig. 8a) and imparted resistance to elevated $[K^+]_e$-mediated suppression of T cell function (Extended Data Fig. 8b). Overexpression or pharmacologic activation of $K_{Ca}3.1$ produced a similar gain of function and resistance to K^+-mediated suppression (Extended Data Fig. 8c, d).

To test whether augmented K^+ efflux improved T cell function *in vivo*, we transferred TCR-transgenic Pmel-1 $CD8^+$ mouse T cells transduced with *Kcna3*, or a control retroviral construct, into B16 tumour-bearing mice. First, we noted that *Kcna3* overexpression in TILs increased Akt–mTOR activation (Fig. 4c) and IFNγ production within tumours (Fig. 4d) and, following brief re-stimulation, *ex vivo* (Extended Data Fig. 8e), without affecting T cell phenotype or number in response to viral infection (Extended Data Fig. 8f–g).

To extend our observations, we tested whether human TILs from multiple cancer types were suppressed by elevated $[K^+]_e$, or alternative treatments that increase $[K^+]_i$, in a PP2A-dependent manner. Consistently, we found that either elevated $[K^+]_e$ or inhibition of endogenous potassium channels with Ba^{2+} increased $[K^+]_i$ and suppressed effector function in a manner that also required intact PP2A function in human TILs (Fig. 4e and Extended Data Fig. 9a, b).

To test whether the gain of function observed as a result of *Kcna3* overexpression resulted from increased ion transport, we generated a non-conducting 'pore dead' construct (*Kcna3*_PD; W389F)[25]. *Kcna3*_PD failed to alter $[K^+]_i$, cytokine production *in vitro* (Fig. 4f, g and Extended Data Fig. 9c) or the effector function of transduced mouse TILs (Extended Data Fig. 9d). Moreover, only intact *Kcna3* resulted in enhanced tumour clearance and host survival in a mouse tumour model (Fig. 4h, i). Collectively, these results indicate that augmenting cellular K^+ efflux can increase the anti-tumour function of adoptively transferred T cells.

In this study, we have shown that cell death within tumours is associated with elevated $[K^+]_e$ at a level that leads to increased $[K^+]_i$ within T cells, silencing of TCR-induced Akt–mTOR phosphorylation and decreased T cell effector function. Although intact PP2A function was required for K^+-mediated suppression of T cell function, K^+ did not directly affect PP2A phosphatase activity (Extended Data Fig. 9e, f), suggesting that a functional intermediate is involved. Investigations into the function of PP2A have identified several endogenous small molecules and metabolites that can variably affect PP2A to increase or decrease its contextual function[26,27]. Future experiments will aim to determine whether $[K^+]_i$ alters the processing, localization or abundance of metabolites that affect PP2A activity. These findings may also shed light on prior observations that changes in $[K^+]_i$ regulate inflammasome activation in macrophages[28] and can control cellular peptide and phospholipid processing[29,30].

Finally, we found that elevated $[K^+]_e$ suppresses T cell effector function and that anti-tumour T cells reprogrammed to express the potassium transporter *Kcna3* exhibited lower $[K^+]_i$ and enhanced effector functions *in vitro* and *in vivo*. These data identify a tumour-induced ionic checkpoint acting upon T cell effector function (Extended Data Fig. 10a–c) and show that manipulating the intracellular ion concentration of anti-tumour T cells can augment disease clearance, with implications for immune-based therapies for cancer.

Online Content Methods, along with any additional Extended Data display items and Source Data, are available in the online version of the paper; references unique to these sections appear only in the online paper.

Received 29 January; accepted 15 August 2016.
Published online 14 September 2016.

1. Mellman, I., Coukos, G. & Dranoff, G. Cancer immunotherapy comes of age. *Nature* **480,** 480–489 (2011).
2. Richards, C. H., Mohammed, Z., Qayyum, T., Horgan, P. G. & McMillan, D. C. The prognostic value of histological tumor necrosis in solid organ malignant disease: a systematic review. *Future Oncol.* **7,** 1223–1235 (2011).
3. Li, G. *et al.* EphB3 suppresses non-small-cell lung cancer metastasis via a PP2A/RACK1/Akt signalling complex. *Nat. Commun.* **3,** 667 (2012).
4. Zhou, P. *et al. In vivo* discovery of immunotherapy targets in the tumour microenvironment. *Nature* **506,** 52–57 (2014).
5. Sitkovsky, M. & Lukashev, D. Regulation of immune cells by local-tissue oxygen tension: HIF1 alpha and adenosine receptors. *Nat. Rev. Immunol.* **5,** 712–721 (2005).
6. Ho, P. C. *et al.* Phosphoenolpyruvate is a metabolic checkpoint of anti-tumor T cell responses. *Cell* **162,** 1217–1228 (2015).
7. Zimmerli, W. & Gallin, J. I. Pus potassium. *Inflammation* **12,** 37–43 (1988).
8. Mirrakhimov, A. E., Ali, A. M., Khan, M. & Barbaryan, A. Tumor Lysis Syndrome in solid tumors: an up to date review of the literature. *Rare Tumors* **6,** 68–76 (2014).
9. Tran, E. *et al.* Cancer immunotherapy based on mutation-specific CD4+ T cells in a patient with epithelial cancer. *Science* **344,** 641–645 (2014).
10. Feske, S. ORAI1 and STIM1 deficiency in human and mice: roles of store-operated Ca2+ entry in the immune system and beyond. *Immunol. Rev.* **231,** 189–209 (2009).
11. Omilusik, K. *et al.* The Ca(v)1.4 calcium channel is a critical regulator of T cell receptor signaling and naive T cell homeostasis. *Immunity* **35,** 349–360 (2011).
12. Li, F. Y. *et al.* Second messenger role for $Mg2^+$ revealed by human T-cell immunodeficiency. *Nature* **475,** 471–476 (2011).
13. Wu, C. *et al.* Induction of pathogenic TH17 cells by inducible salt-sensing kinase SGK1. *Nature* **496,** 513–517 (2013).
14. Wiig, H., Tenstad, O., Iversen, P. O., Kalluri, R. & Bjerkvig, R. Interstitial fluid: the overlooked component of the tumor microenvironment? *Fibrogenesis Tissue Repair* **3,** 12 (2010).
15. Haslene-Hox, H. *et al.* A new method for isolation of interstitial fluid from human solid tumors applied to proteomic analysis of ovarian carcinoma tissue. *PLoS One* **6,** e19217 (2011).
16. Le, D. T. *et al.* PD-1 blockade in tumors with mismatch-repair deficiency. *N. Engl. J. Med.* **372,** 2509–2520 (2015).
17. Robbins, P. F. *et al.* Tumor regression in patients with metastatic synovial cell sarcoma and melanoma using genetically engineered lymphocytes reactive with NY-ESO-1. *J. Clin. Oncol.* **29,** 917–924 (2011).
18. Goldman, D. E. Potential, impedance, and rectification in membranes. *J. Gen. Physiol.* **27,** 37–60 (1943).
19. Hodgkin, A. L. & Huxley, A. F. A quantitative description of membrane current and its application to conduction and excitation in nerve. *J. Physiol.* **117,** 500–544 (1952).
20. Buck, M. D., O'Sullivan, D. & Pearce, E. L. T cell metabolism drives immunity. *J. Exp. Med.* **212,** 1345–1360 (2015).
21. Taffs, R. E., Redegeld, F. A. & Sitkovsky, M. V. Modulation of cytolytic T lymphocyte functions by an inhibitor of serine/threonine phosphatase, okadaic acid. Enhancement of cytolytic T lymphocyte-mediated cytotoxicity. *J. Immunol.* **147,** 722–728 (1991).
22. Liu, Q. H. *et al.* Modulation of Kv channel expression and function by TCR and costimulatory signals during peripheral $CD4^+$ lymphocyte differentiation. *J. Exp. Med.* **196,** 897–909 (2002).
23. Wulff, H. *et al.* The voltage-gated Kv1.3 K^+ channel in effector memory T cells as new target for MS. *J. Clin. Invest.* **111,** 1703–1713 (2003).
24. Cahalan, M. D. & Chandy, K. G. The functional network of ion channels in T lymphocytes. *Immunol. Rev.* **231,** 59–87 (2009).
25. Cidad, P. *et al.* Kv1.3 channels can modulate cell proliferation during phenotypic switch by an ion-flux independent mechanism. *Arterioscler. Thromb. Vasc. Biol.* **32,** 1299–1307 (2012).
26. Voronkov, M., Braithwaite, S. P. & Stock, J. B. Phosphoprotein phosphatase 2A: a novel druggable target for Alzheimer's disease. *Future Med. Chem.* **3,** 821–833 (2011).
27. Hla, T. & Dannenberg, A. J. Sphingolipid signaling in metabolic disorders. *Cell Metab.* **16,** 420–434 (2012).
28. Muñoz-Planillo, R. *et al.* K^+ efflux is the common trigger of NLRP3 inflammasome activation by bacterial toxins and particulate matter. *Immunity* **38,** 1142–1153 (2013).
29. Wolfs, J. L. *et al.* Direct inhibition of phospholipid scrambling activity in erythrocytes by potassium ions. *Cell. Mol. Life Sci.* **66,** 314–323 (2009).
30. Reeves, E. P. *et al.* Killing activity of neutrophils is mediated through activation of proteases by K^+ flux. *Nature* **416,** 291–297 (2002).

Supplementary Information is available in the online version of the paper.

Acknowledgements The research was supported by the Intramural Research Program of the NCI, Wellcome Trust/Royal Society grant 105663/Z/14/Z (R.R.) and UK Biotechnology and Biological Sciences Research Council grant BB/N007794/1 (R.R. and K.O.). We thank S. A. Rosenberg, K. Hanada and K. J. Swartz for their valuable discussions and intellectual input, A. Mixon and S. Farid for expertise with cell sorting and G. McMullen for expertise with mouse handling.

Author Contributions R.E., S.V., R.R., J.H.P., C.A.K., and N.P.R. wrote the manuscript. R.E. designed all experiments and carried them all out except those shown in Extended Data (ED) Figs 1c, d, 9e, f. S.V. designed and carried out experiments shown in Figs 1h, i, 4h, i and ED Figs 1c, d, 2a, b, 3e, 8d, f, g, 9e, f. R.R. designed experiments shown in Figs 1a–d, 2a, b, e, 3a, c, k, 4d, f–i and ED Figs 1b, 2c, d, 3c, e, 4e–g, 5b, e, 7c–f, 8a, e–g; N.P.R. designed all experiments. D.C. designed experiments shown in Figs 3b, 4b, and ED Figs 2c, d, 4c–g and 8e–g. C.A.K. designed experiments shown in Figs 1b, c, j, 2, 3c, 4c, e, h, i and ED Figs 2e–h, 8e–g and 9b. J.H.P. designed experiments shown in Fig. 3h–m and ED Figs 2c, d, 7a, b. Z.Y. designed and carried out experiments shown in Fig. 4h, 4i and ED Fig 8f and g. D.P. designed experiments shown in Figs 2a–c, 4h, i, and ED Fig. 3a, c. T.Y. edited the manuscript, provided reagents and designed experiments shown in Fig. 1j and ED Figs 8f, 8g. K.O. and V.C. provided reagents, designed, and carried out experiments shown in Fig. 2h. A.G. provided reagents and designed experiments shown in Fig. 1j and ED Fig. 2f–h. M.S. designed and carried out experiments shown in ED Fig. 4c, 4d. S.P. designed experiments shown in Figs 3a, 1h, i and ED Figs 1c, d, 2a, b. G.C.G. designed experiments shown in Fig. 2d–g and ED Fig. 2b–d and carried out experiments shown in ED Fig. 3c. D.S.S. and W.M.L. contributed reagents for experiments shown in Fig. 1b and ED Fig. 1b.

Author Information RNA-sequencing raw data files are deposited in the Gene Expression Omnibus database with the accession number GSE84996. Reprints and permissions information is available at www.nature.com/reprints. The authors declare no competing financial interests. Readers are welcome to comment on the online version of the paper. Correspondence and requests for materials should be addressed to R.E. (eil@ohsu.edu) or N.P.R. (restifon@mail.nih.gov).

Reviewer Information *Nature* thanks G. Chandy and the other anonymous reviewer(s) for their contribution to the peer review of this work.

METHODS

Study approval. Animal experiments were conducted with the approval of the NCI and NIAMS Animal Use and Care Committees. All NIH cancer patients providing human samples were enrolled in clinical trials approved by the NIH Clinical Center and NCI institutional review boards. Each patient signed an informed consent form and received a patient information form before participation.

Mice and cell lines. Pmel-1 (B6.Cg-/Cy Tg [TcraTcrb] 8Rest/J), *Rag2*$^{-/-}$, OT-II (B6.Cg-Tg (TcraTcrb)425Cbn/J), and C57BL/6 mice were obtained from Jackson Laboratory. C57BL/6 male mice of 6–8 weeks of age were used as recipient hosts for adoptive transfer unless otherwise indicated. We crossed Pmel-1 with Ly5.1 mice (B6.SJL-Ptprc^a*Pepc*^{b}/BoyJ) to obtain Pmel-1 Ly5.1 mice. We crossed OT-II with *Rag2*$^{-/-}$ to obtain OT-II *Rag*$^{-/-}$ mice. All mice were maintained under specific pathogen-free conditions. B16 (H-2D^b), a mouse melanoma, transduced as previously described[31] to express glycoprotein 100 (gp100) with human residues at positions 25–27; EGS to KVP. The Mel624 human melanoma-derived cell line was a gift of S.A.R. Platinum-E ecotropic packaging cells were obtained from Cell Biolabs. HLA-A*0201$^+$ NY-ESO-1$^+$ A375 cells were obtained from ATCC. Cell lines were maintained in DMEM with 10% FBS, 1% glutamine and 1% penicillin–streptomycin.

Cell line authentication. Platinum-E cells were obtained from Cell Biolabs following authentication and validation as being mycoplasma free. A375 cells were obtained from ATCC following authentication and validation as being mycoplasma free. Mel624 was authenticated as previously described[17]. Authenticated B16 was obtained from the National Cancer Institute Tumour Repository and validated as being mycoplasma free via a PCR-based assay.

Statistical analysis. Data were compared using either a two-tailed Student's *t*-test corrected for multiple comparisons by a Bonferroni adjustment or repeated measures two-way ANOVA, as indicated. Where necessary, the Shapiro–Wilk test was used to test for normality of the underlying sample distribution. Experimental sample sizes were chosen using power calculations with preliminary experiments or were based on previous experience of variability in similar experiments. Samples that had undergone technical failure during processing were excluded from analyses. The Kolmogorov–Smirnov test was used to evaluate the significance between different distributions. For adoptive transfer experiments, recipient mice were randomized before cell transfer. The products of perpendicular tumour diameters were plotted as the mean ± s.e.m. for each data point, and tumour treatment graphs were compared by using the Wilcoxon rank sum test and analysis of animal survival was assessed using a log-rank test. In all cases, *P* values of less than 0.05 were considered significant. Statistics were calculated using GraphPad Prism 7 software (GraphPad Software Inc.).

Electrolyte analysis of serum and interstitial fluid. We used a previously reported method to isolate tissue interstitial fluid via a centrifugation method[6,14,15]. Briefly, *en bloc* tissue was harvested, placed on triple-layered 10-μm nylon mesh and spun at <50*g* for 5 min to remove surface liquid. Next, samples were centrifuged at 400*g*, a previously validated speed at which intracellular contents are not liberated[14,15], for an additional 10 min Flow-through from this step was retained as interstitial fluid and assayed for indicated electrolyte concentrations in a blinded fashion within the NIH Central Clinical Chemistry Laboratory using auto analyser ion selective electrode quantification (Cobas 6000; US Diagnostics)[32].

External solution formulations. Unless otherwise indicated, re-activation of cells in elevated $[K^+]_e$ was performed with an isotonic RPMI formulation with an additional 40 mM of potassium for mouse cells and 50 mM for human cells in comparison to the control condition medium. In principal this medium was produced by obtaining a custom formulation of RPMI 1640 from Gibco that was devoid of NaCl. For control conditions, this medium was reconstituted with NaCl to produce a solution equimolar to standard RPMI. Thus, the final inorganic salt concentrations for the control condition were identical to those in RPMI 1640 (Gibco) in mM: NaCl 103.4, $NaHC0_3$ 23.8, Na_2PO_4 5.6, KCl 5.3, $MgSO_4$ 0.4 and $Ca(NO_3)_2$ 0.4. For isotonic medium containing an additional 40 mM KCl, this medium was reconstituted with a combination of NaCl and KCl such that the final inorganic salt concentrations, in mM, were: NaCl 63.4, $NaHC0_3$ 23.8, Na_2PO_4 5.6, KCl 45.3, $MgSO_4$ 0.4 and $Ca(NO_3)_2$ 0.4. For 40 mM hypertonic NaCl the final inorganic salt concentrations were, in mM: NaCl 143.4, $NaHC0_3$ 23.8, Na_2PO_4 5.6, KCl 5.3, $MgSO_4$ 0.4 and $Ca(NO_3)_2$ 0.4. For 40 mM hypertonic KCl the final inorganic salt concentrations were, in mM: KCl 143.4, $NaHC0_3$ 23.8, Na_2HPO4 5.6, KCl 5.3, $MgSO_4$ 0.4 and $Ca(NO_3)_2$ 0.4. All other additives in RPMI 1640 (vitamins, amino acids, glutathione, phenol red, etc) were unchanged in quality or quantity.

T cell TCR-induced Ca^{2+} experiments were carried out in a combination of NaCl-depleted RPMI 1640 reconstituted with NaCl or KCl and HBSS with Ca^{2+} and Mg^{2+} and without phenol red (Gibco). As such, the final inorganic salt concentrations in control conditions were, in mM: NaCl 120.6, $NaHC0_3$ 13.9, Na_2PO_4 2.9, KCl 5.3, $MgSO_4$ 0.4, $Ca(NO_3)_2$) 0.2, $CaCl_2$ 0.63, KH_2PO_4 0.22, $MgCl_2$ 0.25 and D-glucose 8.3. In the same experiment the concentrations of inorganic salts, in mM, in the conditions with elevated $[K^+]_e$ were: NaCl 80.6, $NaHC0_3$ 13.9, Na_2PO_4 2.9, KCl 45.3, $MgSO_4$ 0.4, $Ca(NO_3)_2$ 0.2, $CaCl_2$ 0.63, KH_2PO_4 0.22, $MgCl_2$ 0.25 and D-glucose 8.3. As this final solution was a combination of HBSS and RPMI 1640 it contained all of the non-inorganic salt additives (vitamins, amino acids, glutathione, phenol red) normally in standard RPMI 1640, as reported in the publically available Gibco formulation, at half of the original concentration.

Generation and activation of effector T cells. *In vitro* activation of T cells was carried out either by negative enrichment (Miltenyi Biotec) of CD8$^+$ T cells from C57BL/6 mice followed by activation using immobilized anti-CD3 (145-2C11; eBioscience) and anti-CD28 (37-51; eBioscience) along with expansion in culture medium containing IL-2 for 4–5 days, or via isolation of Pmel-1 Ly5.1 mouse whole splenocytes followed by stimulation *in vitro* with 1 μM human glycoprotein 100 nine-mer peptide ($hgp100_{25–33}$) peptide and expansion in culture medium containing IL-2 for 4–5 days. For analysis of T cell effector function, these cells were then stimulated on day 4 or 5 of culture in the indicated conditions for 5 h with anti-CD3 and -CD28 without IL-2 in the presence of brefeldin A and monesin (BD Biosciences). For assaying co-inhibitory signalling, during PD-L1-based co-inhibition, PD-L1-IgG2a (R&D) was conjugated along with anti-CD3 and anti-CD28 antibodies (eBioscience) and control IgG2a (R&D) onto M-450 Epoxy Dynabeads (Thermo Fisher) at a ratio of (1:1:2:6) for (anti-CD3:anti-CD28:PD-L1-IgG2a:IgG2a) for a total of 5 μg ml^{-1} protein per 2×10^6 beads overnight at 4 °C. For comparative control conditions IgG2a was replaced by PD-L1 to control for bead loading. These beads were then incubated with effector CD8$^+$ T cells at a ratio of 1:1 in the indicated conditions for 5 h. For CTLA-4 based co-inhibition, anti-CD3, anti-CD28, and CTLA-4-IgG2a (R&D) or IgG2a (R&D) were coated onto tissue culture-treated 96-well plates at a concentration of 5 μg ml^{-1} (in a fashion similar to standard immobilized antibody-based stimulation) for each reagent overnight at 4 °C. For assaying neoantigen specific reactivity, human TILs from NCI-14-C-0062, generated as described below, were re-activated for 5 h with autologous pre-activated B cells that were pulsed with the indicated wild-type or neo-antigen peptides as described below. Transduced human peripheral blood lymphocytes were co-cultured with the A375 patient-derived melanoma tumour line HLA-A*0201$^+$ and positive for NY-ESO-1 expression[33], at a ratio of 1 T cell to 3 tumour cells in the presence of brefeldin A and monesin (BD Biosciences) for 5 h. For analysis of human CD8$^+$ TILs from varied histologies in the presence or absence of elevated K^+ or Ba^{2+}, TILs were first grown from tumour fragments cultured in 6,000 IU ml^{-1} IL-2 in a 1-to-1 mixture of RPMI 1640 and AIM-V, supplemented with 5% in-house human serum 100 μg ml^{-1}streptomycin and 100 μg ml^{-1} penicillin, 2 mM L-glutamine, 10 μg ml^{-1} gentamicin, for approximately 14 days per standard operating GMP protocols practiced by the Surgery Branch[34]. These T cells were then subjected to a rapid expansion protocol (REP) using irradiated peripheral blood mononuclear cells (PBMC) at a ratio of 1 to 300 in the same complete medium with 30 ng ml^{-1} OKT3 in preparation for subsequent patient transfer. These cells were activated via immobilized anti-CD3 and anti-CD28 in the presence of K^+, Ba^{2+}, and/or okadaic acid (OA) as indicated. For experiments Naive mouse CD4$^+$ cells were obtained by isolating splenocytes from 6–10 week-old OT-II *Rag*$^{-/-}$ mice and subjected to negative selection of naive CD4$^+$ T cells (Stemcell Technologies). These naive cells were activated with immobilized anti-CD3 and anti-CD28 (5 μg ml^{-1} each) in medium for 2 days followed by an additional 2 days on blank plates with relevant polarizing cytokines present during the entire duration of the 4-day culture: T_H1 conditions (IL-12 10 ng ml^{-1} or as indicated, R&D Systems) T_H17 conditions (IL-6 (20 ng ml^{-1}, R&D Systems), human TGF-β1 (1 ng ml^{-1}, R&D Systems), anti-IFNγ neutralizing antibodies (10 μg ml^{-1}), IL-1β (10 ng ml^{-1}), or iT_{reg} conditions (human TGF-β1 200 pg ml^{-1}) as indicated.

For selected experiments as indicated cells were treated with the PP2A inhibitor okadaic acid at a concentration of 200 nM (mouse CD8$^+$ T cells) or 125 nM (human CD8$^+$ TIL), the ionophore gramicidin (0.75 or 1.5 μM), the inhibitor of the Na^+,K^+-ATPase, ouabain 125 μM (pre-incubated for 30 min), the K_{Ca}3.1 activator 1-EBIO (50 μM), or the ionophore valinomycin (2 μM).

RNA purification, quantitative real-time RT–PCR, RNA-sequencing and bioinformatic analysis. RNA sequencing was performed and analysed as described previously[35]. CD8$^+$62L$^+$ C57BL/6 splenocytes were FACS sorted from 6–8-week-old mice in biological triplicate and activated with anti-CD3 and -CD28 for 48 h in IL-2 100 IU ml^{-1} and cultured in RPMI complete medium for an additional 72 h. Cells were then subjected to ficoll density separation to isolate live cells, placed in complete medium without IL-2 in the presence or absence of elevated $[K^+]_e$, and either re-stimulated with anti-CD3 and -CD28 or kept in complete medium for 2 h with no stimulation (No stim). Cellular RNA was preserved with RNA*later* (Qiagen) and purified with the RNeasy Plus Mini Kit (Qiagen). RNA was subsequently used to prepare RNA-seq libraries by using TruSeq SRRNA sample prep kit (FC-122-1001, Illumina) according to the manufacturer's instructions. The libraries were sequenced for 150 bp (paired-end) using a NextSeq500 sequencer

(Illumina). Sequence reads from each cDNA library were mapped onto the mouse genome build mm9 by using TopHat, and the mapped data was then processed by Cufflinks[36]. The obtained data was normalized based on RPKM (reads per kilobase exon model per million mapped reads). To define differentially regulated genes, we used a 1.5-fold change difference between treatment groups. Real-time RT–PCR was performed for genes following cDNA generation by reverse transcription (Applied Biosystems) with primers from Applied Biosystems by Prism 7900HT (Applied Biosystems).

Extracellular acidification rate and basal oxygen consumption rate. Oxygen consumption rates (OCR) and extracellular acidification rates (ECAR) were measured following re-stimulation of T cells using anti-CD3/CD28 Dynabeads (Invitrogen) in a 0.8:1 ratio at 37 °C using an XF24 extracellular analyser (Seahorse Bioscience) as previously described[37] in the indicated conditions. OCR and ECAR were measured in XF medium (non-buffered RPMI 1640 containing 25 mM glucose, 2 mM L-glutamine, and 1 mM sodium pyruvate) in a 1:1 mixture with tonicity-controlled, additive-free standard RPMI 1640 with normal or elevated $[K^+]$ under basal conditions and in response to 1 μM oligomycin, 2 μM fluoro-carbonyl cyanide phenylhydrazone (FCCP) or 100 nM rotenone with 1 μM antimycin A (Sigma).

Intracellular cytokine staining, phosphoflow and flow cytometry. Suspensions containing T cells were stained with a fixable live/dead stain (Invitrogen) in PBS followed by surface antibody staining in FACS buffer (PBS with 0.5% BSA and 0.1% sodium azide). For intracellular cytokine staining, cells were stained for intracellular molecules following fixation and permeabilization. For phosphostaining BD PhosFlow reagents were used and fixation and permeabilization protocols were carried out according to the manufacturer's protocols. After washing, cells were stained with antibody-fluorochrome conjugates for the indicated phosphorylated proteins ($pZap70^{Y319}$ (BD Biosciences); all other phospho-antibodies were purchased from Cell Signaling). Antibodies for surface staining and intracellular cytokine staining were purchased from BD Biosciences and eBiosciences. For determination of cytoplasmic V_m cells were incubated in 2 μM $DiSBAC_4 3$ (Invitrogen) in conditions as indicated for 60 min before evaluation. For determination of $[K^+]_i$, cells were loaded with the potassium-sensitive dye Asante Green-4 (TEFLabs) with PowerLoad (Invitrogen) per the manufacturer's protocols. All experiments were conducted on a BD Fortessa flow cytometer (Becton Dickinson) and analysed with FlowJo software.

Identification and purification of mutation-specific TILs. Cancer-specific mutations and TILs targeted against those mutations from patients with metastatic melanoma were identified as previously described[38]. Briefly, patients were enrolled on a clinical protocol (NCI-14-C-0062). Whole-exomic sequencing (WES) was performed on tumour tissue and normal peripheral blood cells by Personal Genome Diagnostics (PGDx) and the data were aligned to genome build hg18. A viable metastatic tumour deposit was selected for resection as a source for TILs. The resected *en bloc* tumour was subjected to mechanical disruption using a GentleMACS Dissociator (Miltenyi Biotec). The bulk tumour digest was cultured in complete medium without IL-2 or other cytokines overnight. The following day $CD3^+PD\text{-}1^+$ T cells were FACS sorted using a BD FACSJazz flow cytometer. These sorted T cells were then subjected to a rapid expansion protocol (REP) using irradiated PBMC at a ratio of 1 to 300 in 50/50 medium (1-to-1 mixture of RPMI 1640 and AIM-V, supplemented with 5% in-house human serum, 100 U ml^{-1}penicillin, 100 μg ml^{-1}streptomycin, 2 mM L-glutamine and 10 μg ml^{-1}gentamicin), 3,000 IU ml^{-1} IL-2, and 30 ng ml^{-1} OKT3 antibody (Miltenyi Biotec) for approximately 14 days. At the conclusion of the first REP T cells were screened and FACS sort-enriched with the BD FACSJazz based on 41BB positivity[38], against tandem mini-gene (TMG) constructs encoding for tumour specific mutations identified by WES for each patient and tumour, as described above[9,38,39]. These enriched neo-antigen-specific T cells were then expanded via a second REP. At the conclusion of the second REP T cells were activated with peptide pulsed (at 1:3; effector:target) autologous CD40L-stimulated B cells with either 10 μg ml^{-1} of the full length 23-mer mutated or wild peptide (patient A) or 1 μg ml^{-1} of the minimal epitope (patients B, C) in the indicated conditions.

Retroviral transduction. Platinum-E ecotropic packaging cells (Cell Biolabs) were plated one day before transfections on poly-D-lysine-coated 10-cm plates (Corning) at a concentration of 6×10^6 cells per plate. Packaging cells were transfected with 20 μg of retroviral plasmid DNA encoding MSGV-Thy1.1, MSGV-*Kcna3*-Thy1.1, MSGV-*Kcna3*-Thy1.1 (W389F) (referred to as *Kcna3_PD*)[25,40], MSGV-*Ppp2r1a*(K416E)-Thy1.1 (referred to as PP2A_DN[41,42]), MSCV-IRES-Thy1.1 (pMIT), or pMIT *Akt1*-CA[43] where indicated along with 6 μg pCL-Eco plasmid DNA using 60 μl Lipofectamine 2000 in OptiMEM (Invitrogen) for 8 h in antibiotic-free medium. Medium was replaced 8 h after transfection and cells were incubated for a further 48 h. Retroviral supernatants were then collected and spun at 2,000*g* for 2 h at 32 °C onto 24-well non-tissue-culture-treated plates coated overnight in Retronectin (Takara Bio). For *in vivo* experiments live cells were isolated via ficoll density separation (Cedarlane) and subjected to positive selection via CD90.1-microbead column enrichment according to the manufacturer's protocol (Miltenyi Biotec) before transfer, yielding a $CD8^+$ T cell population 70–95% $Thy1.1^+$ before transfer. For retroviral transduction of human peripheral blood lymphocytes (PBL) with the NY-ESO-1 TCR, patients with metastatic melanoma on clinical protocol NCI-13-C-0214 were subjected to leukapheresis and the PBL of these patients were transduced with a MSGV1 backbone encoding the NY-ESO-1 mouse-derived TCR as previously described[17]. After primary transduction and culture (10 days), these cells were then further expanded via a REP as described above (days 10–23) and subsequently assayed for target-specific effector function in the indicated conditions.

Adoptive cell transfer (ACT) and tumour immunotherapy. For immunotherapy, C57BL/6 were implanted with subcutaneous B16 melanoma (5×10^5 cells). At the time of adoptive cell transfer (ACT), 10 days after tumour implantation, mice ($n \geq 5$ for all groups) were sub-lethally irradiated (600 cGy), randomized, and injected intravenously with 5×10^5 Pmel-1 Ly5.1 cells transduced with control- or *Kcna3*-expressing retrovirus and received intraperitoneal injections of IL-2 in PBS (6×10^4 IU per 0.5 ml) once daily for 3 days starting on the day of cell transfer. Tumours were blindly measured using digital callipers. Tumour size was measured in a blinded fashion approximately every two days after transfer and tumour area was calculated as length × width of the tumour. Mice with tumours greater than 400 mm^2 were killed. The products of the perpendicular tumour diameters are presented as mean ± s.e.m. at the indicated times after ACT. For functional analysis of transferred Pmel-1cells, B16 tumour-bearing mice received Pmel-1 cells as above, and 6–8 days following cell transfer mice were injected with 500 μl of 0.5 mg ml^{-1} brefeldin A (Sigma) and 6 h later tumours were harvested and processed for live/dead, surface, fixation, and intracellular staining for direct *in vivo* IFNγ capture[44]. For *ex vivo* restimulation, tumours were harvested and processed as above, red cells were lysed with ACK lysis buffer for 2 min at room temperature, then cell suspensions were subjected to live-cell isolation via ficoll density gradient separation (CedarLane) and stimulated in medium containing leukocyte activation cocktail with Golgiplug (BD biosciences) for 4 h at a final concentration of 2 μl ml^{-1}.

Viral infection and kinetic analysis. For assessing the response of $CD8^+$ T cells to acute viral infection, 5×10^5 transduced and $Thy1.1^+$ enriched Pmel-1 Ly5.1 $CD8^+$ T cells were transferred into recipient Thy1.2 Ly5.2 C57BL/6 mice. Immediately following transfer, mice were infected with rhgp100 1×10^7 plaque-forming units (PFU). At the indicated time points following transfer, recipient mouse blood was obtained via sub-mandibular venipuncture and analysis for phenotype and enumeration of the congenically identified transferred cells was carried out.

T cell receptor (TCR) crosslinking, western blots. As described previously[45], to induce TCR crosslinking *in vitro* generated T cells were rested overnight in the absence of IL-2, subsequently subjected to live cell isolation via ficoll density gradient separation and pre-incubated with soluble anti-CD3- and anti-CD28-biotin, appropriate surface antibodies and pharmacologic inhibitors where indicated in additive-free RPMI 1640 at 4 °C. Cells were then washed, brought up to 37 °C, and linked via the addition of streptavidin in the indicated conditions. For western blots, at the indicated time points following cross-linking, cells were lysed by the addition of 95 °C 2 × Laemmli sample buffer with 2-mercaptoethanol (Bio-Rad Laboratories) and sonicated for 40 s at 10% intensity before gel loading. For $K_v1.3$ protein analysis, $Thy1.1^+$ enriched T cells were lysed in 1× RIPA buffer (Thermo Fisher) with protease and phosphatase inhibitors (Roche). Western blotting was performed using TGX reagents (Bio-Rad Laboratories) and protocols on PVDF paper. Following transfer, blots were blocked with 5% BSA then incubated with antibodies against phospho-tyrosine (4G10; EMD Millipore), pAkt-T308, total Akt, β-actin, Akt-substrate, or phospho-threonine with appropriate HRP-conjugated or Alexa 647-conjugated secondary antibodies (Cell Signaling Technology) or anti-$K_v1.3$ (NeuroMab). For HRP-conjugated secondary antibodies blots were developed using chemiluminescence (Thermo Fisher) and gel images were captured with the Gel Doc XRS (Bio-Rad Laboratories). For PI3K activity, cells were fixed at the indicated time points by the 1:1 addition of a mixed lysis solution containing 30 mM HCl, 65% methanol and 30% chloroform, maintained at −80 °C, then processed and analysed as previously described[46].

T cell receptor induced calcium influx. T cells were isolated and primed as above. Prior to analysis cells were rested in IL-2-free complete RPMI 1640 for at least 8 h. Cells were loaded with 1 μM Fluo3-AM and 1 μM Fura Red-AM (Invitrogen) for 30 min at 37 °C in HBSS with Ca^{2+}, Mg^{2+} and 2% FCS, washed twice and then resuspended in HBSS with anti-CD3- and -CD28-biotin conjugates (eBioscience) and a live/dead stain (Invitrogen). For flow cytometry analysis, samples were resuspended in pre-warmed 37 °C 1:1 mixtures of HBSS and isotonic normokalaemic or hyperkalaemic additive-free RPMI (as described above), a baseline measurement was recorded for 20 s, followed by the addition of streptavidin (Invitrogen) to a final concentration of 20 μg ml^{-1} to induce TCR

cross-linking and Ca^{2+} influx. Kinetic analyses were performed with the FlowJo software package (TreeStar).

shRNA mediated *Ppp2r2d* knockdown. A pLKO-Thy1.1 construct targeting *Ppp2r2d* was provided by P.Z. and K.W.W. and lentiviral particles were generated using their protocol[4]. Bone marrow (BM) cells were collected from the femurs and tibiae of 6–8-week-old donor mice. After red blood cell lysis, haematopoietic stem and progenitor cells were enriched by autoMACS depletion of lineage-positive cells using the Lineage Cell Depletion Kit (Miltenyi Biotec) for BM cells. Negatively selected cells were cultured in chemically defined serum-free medium X-vivo 10 with gentamicin (Lonza) supplemented with L-glutamine (1×) (Gibco), β-mercaptoethanol (50 mM), mouse recombinant SCF (50 ng ml^{-1}), IL-6 (10 ng ml^{-1}), IL-3 (5 ng ml^{-1}), FLT-3L (5 ng ml^{-1}) and IL-7 (5 ng ml^{-1}) (Peprotech). The following day, these lineage-depleted BM cells were transduced by spin-infection at 32 °C degrees, 2,000 r.p.m for 90 min in the presence of lentiviral supernatant and 5 μg ml^{-1}polybrene (Sigma-Aldrich). Cells were incubated for another 2–4 h before tail vein injection into *Rag2*$^{-/-}$ lethally irradiated (1,000 cGy) recipient mice at 1–2 × 10^6 cells per mouse in 500 μl sterile PBS. $CD8^+Thy1.1^+CD44^+CD62L^+$ cells were FACS sorted 6–8 weeks after adoptive transfer, activated, and assayed as above.

PP2A phosphatase assay. PP2A activity was evaluated after immunoprecipitation using a malachite green phosphatase assay kit as per the manufacturer's instructions (EMD Millipore).

31. Acquavella, N. *et al.* Type I cytokines synergize with oncogene inhibition to induce tumor growth arrest. *Cancer Immunol. Res.* **3,** 37–47 (2015).
32. Budak, Y. U., Huysal, K. & Polat, M. Use of a blood gas analyzer and a laboratory autoanalyzer in routine practice to measure electrolytes in intensive care unit patients. *BMC Anesthesiol.* **12,** 17 (2012).
33. Wargo, J. A. *et al.* Recognition of NY-ESO-1$^+$ tumor cells by engineered lymphocytes is enhanced by improved vector design and epigenetic modulation of tumor antigen expression. *Cancer Immunol. Immunother.* **58,** 383–394 (2009).
34. Goff, S. L. *et al.* Randomized, prospective evaluation comparing intensity of lymphodepletion before adoptive transfer of tumor-infiltrating lymphocytes for patients with metastatic melanoma. *J. Clin. Oncol.* **34,** 2389–2397 (2016).
35. Vahedi, G. *et al.* STATs shape the active enhancer landscape of T cell populations. *Cell* **151,** 981–993 (2012).
36. Trapnell, C. *et al.* Transcript assembly and quantification by RNA-Seq reveals unannotated transcripts and isoform switching during cell differentiation. *Nat. Biotechnol.* **28,** 511–515 (2010).
37. van der Windt, G. J. *et al.* Mitochondrial respiratory capacity is a critical regulator of $CD8^+$ T cell memory development. *Immunity* **36,** 68–78 (2012).
38. Tran, E. *et al.* Immunogenicity of somatic mutations in human gastrointestinal cancers. *Science* **350,** 1387–1390 (2015).
39. Lu, Y. C. *et al.* Efficient identification of mutated cancer antigens recognized by T cells associated with durable tumor regressions. *Clin. Cancer Res.* **20,** 3401–3410 (2014).
40. Jiménez-Pérez, L. *et al.* Molecular determinants of Kv1.3 potassium channels-induced proliferation. *J. Biol. Chem.* **291,** 3569–3580 (2016).
41. Turowski, P., Favre, B., Campbell, K. S., Lamb, N. J. & Hemmings, B. A. Modulation of the enzymatic properties of protein phosphatase 2A catalytic subunit by the recombinant 65-kDa regulatory subunit PR65α. *Eur. J. Biochem.* **248,** 200–208 (1997).
42. Xing, Y. *et al.* Structure of protein phosphatase 2A core enzyme bound to tumor-inducing toxins. *Cell* **127,** 341–353 (2006).
43. Hand, T. W. *et al.* Differential effects of STAT5 and PI3K/AKT signaling on effector and memory CD8 T-cell survival. *Proc. Natl Acad. Sci. USA* **107,** 16601–16606 (2010).
44. Liu, F. & Whitton, J. L. Cutting edge: re-evaluating the *in vivo* cytokine responses of CD8+ T cells during primary and secondary viral infections. *J. Immunol.* **174,** 5936–5940 (2005).
45. Palmer, D. C. *et al.* Cish actively silences TCR signaling in $CD8^+$ T cells to maintain tumor tolerance. *J. Exp. Med.* **212,** 2095–2113 (2015).
46. Clark, J. *et al.* Quantification of PtdInsP3 molecular species in cells and tissues by mass spectrometry. *Nat. Methods* **8,** 267–272 (2011).

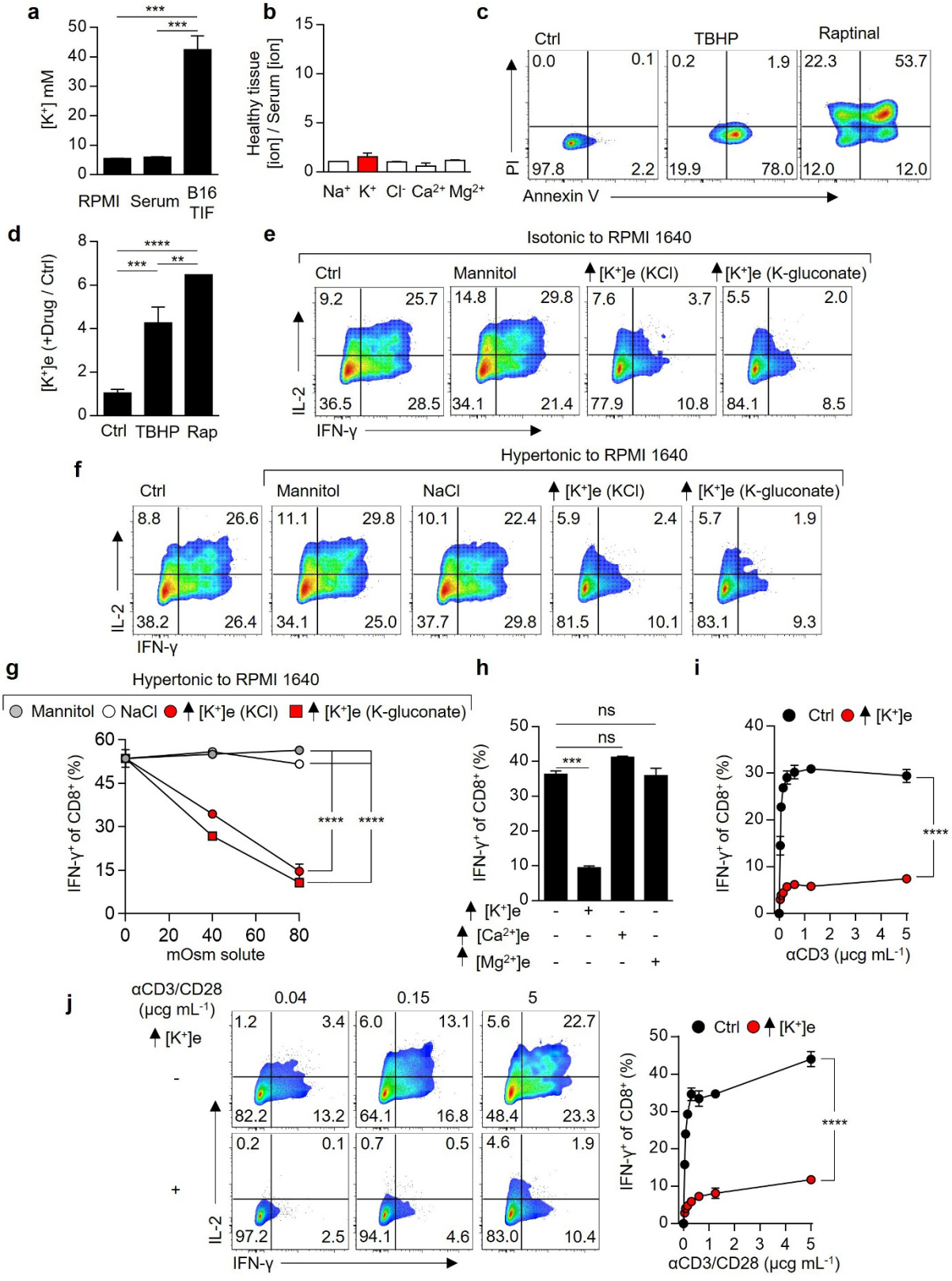

Extended Data Figure 1 | See next page for caption.

Extended Data Figure 1 | Extracellular K^+ release from apoptotic and necrotic cells inhibits T cell effector function. a, $[K^+]$ in TIF, RPMI medium and mouse serum. **b**, Ratio of indicated ions in normal human tissue in comparison to serum measured on the day of tissue collection in cancer patients undergoing resection of nearby cancers originating from the same tissue type. **c**, Representative flow cytometry plots of B16 melanoma tumour cells following the indicated treatment. **d**, $[K^+]_e$ quantification following the indicated treatment. **e**, **f**, Representative flow cytometry plots of anti-CD3/CD28-stimulated $CD8^+$ T cells cultured in isotonic or hypertonic RPMI medium in the indicated conditions. **g**, Quantification of **f**. **h**, Quantification of cytokine production by $CD8^+$ T cells following stimulation in the indicated conditions; elevated Ca^{2+} and Mg^{2+} are 2 mM, in comparison to 0.4 mM for control conditions. **i**, Cytokine production by T cells across a titration of anti-CD3 in the indicated conditions. **j**, Representative flow cytometry plots and quantification following anti-CD3/CD28 titration-based activation of $CD8^+$ T cells in the indicated conditions. Centre values and error bars represent mean ± s.e.m. $*P < 0.05$; $**P < 0.01$; $***P < 0.001$; $****P < 0.0001$ between selected relevant comparisons, two-tailed Student's *t*-tests (**a**–**d**, **h**), two-way ANOVA (**g**, **i**, **j**). **a**, $n =$ at least three biological replicates; **b**, $n = 5$ biological replicates; **c**, **d**, $n = 4$ experimental replicates; **e**–**j**, $n = 3$ culture replicates per condition; **c**–**j**, representative of at least two independent experiments.

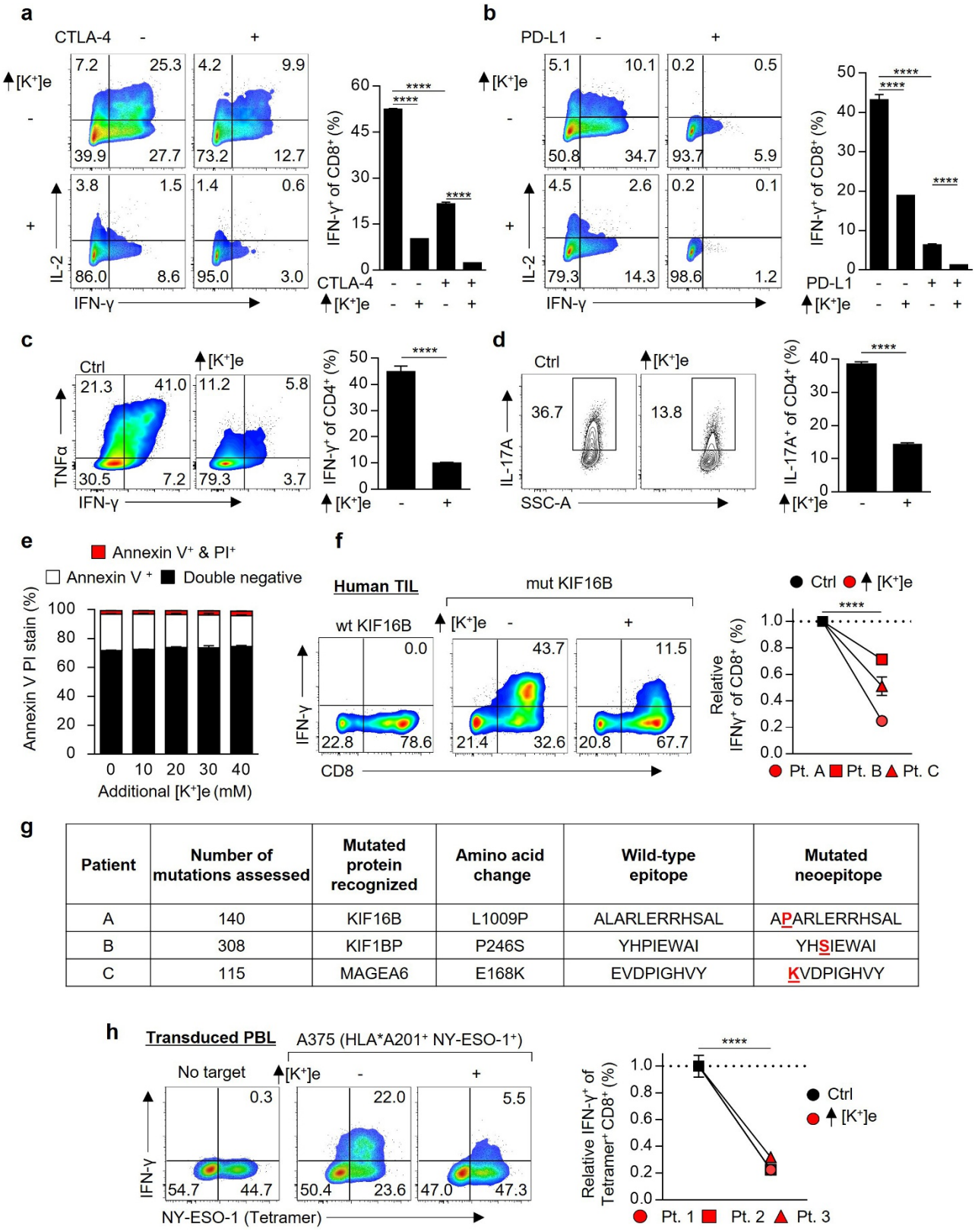

Patient	Number of mutations assessed	Mutated protein recognized	Amino acid change	Wild-type epitope	Mutated neoepitope
A	140	KIF16B	L1009P	ALARLERRHSAL	APARLERRHSAL
B	308	KIF1BP	P246S	YHPIEWAI	YHSIEWAI
C	115	MAGEA6	E168K	EVDPIGHVY	KVDPIGHVY

Extended Data Figure 2 | See next page for caption.

Extended Data Figure 2 | Potassium-induced T cell suppression is functionally non-redundant with CTLA-4 and PD-L1 co-inhibitory signals and is present in TIL neoantigen responses. a, **b**, IFNγ^+ from $CD8^+$cells in the indicated conditions. **c**, **d**, Flow cytometry analysis of cytokine production by $CD4^+$ T cells polarized under T_H1 (**c**) or T_H17 (**d**) conditions and subsequently re-activated via immobilized anti-CD3/CD28 in the indicated experimental conditions. **e**, Annexin V and propidium iodide (PI) staining following activation of primed $CD8^+$ T cells in the indicated conditions. **f**, Representative flow cytometry plots and quantification of human neo-antigen-selected TILs from three patients (Pt.) stimulated in the indicated conditions with cognate mutated (mut) neo-antigen peptide-pulsed target cells (autologous B cells). **g**, Relevant somatic mutation-induced neoepitopes for three patients A–C in **f**. **h**, Representative flow cytometry and quantification of peripheral blood leukocytes from three patients transduced with an HLA*A201-restricted NY-ESO-1 TCR were assayed in the indicated conditions for IFNγ production. Additional $[K^+]_e = 40$ mM for **a**–**e**, $[K^+]_e = 50$ mM for **f**, **h**; $n = 3$ culture replicates per patient per data point, representative of two independent experiments. Centre values and error bars represent mean ± s.e.m. $^*P < 0.05$; $^{**}P < 0.01$; $^{***}P < 0.001$; $^{****}P < 0.0001$, two-tailed Student's *t*-tests (**a**–**h**). **a**–**h**, $n =$ at least three culture replicates per data point and representative of at least two independent experiments.

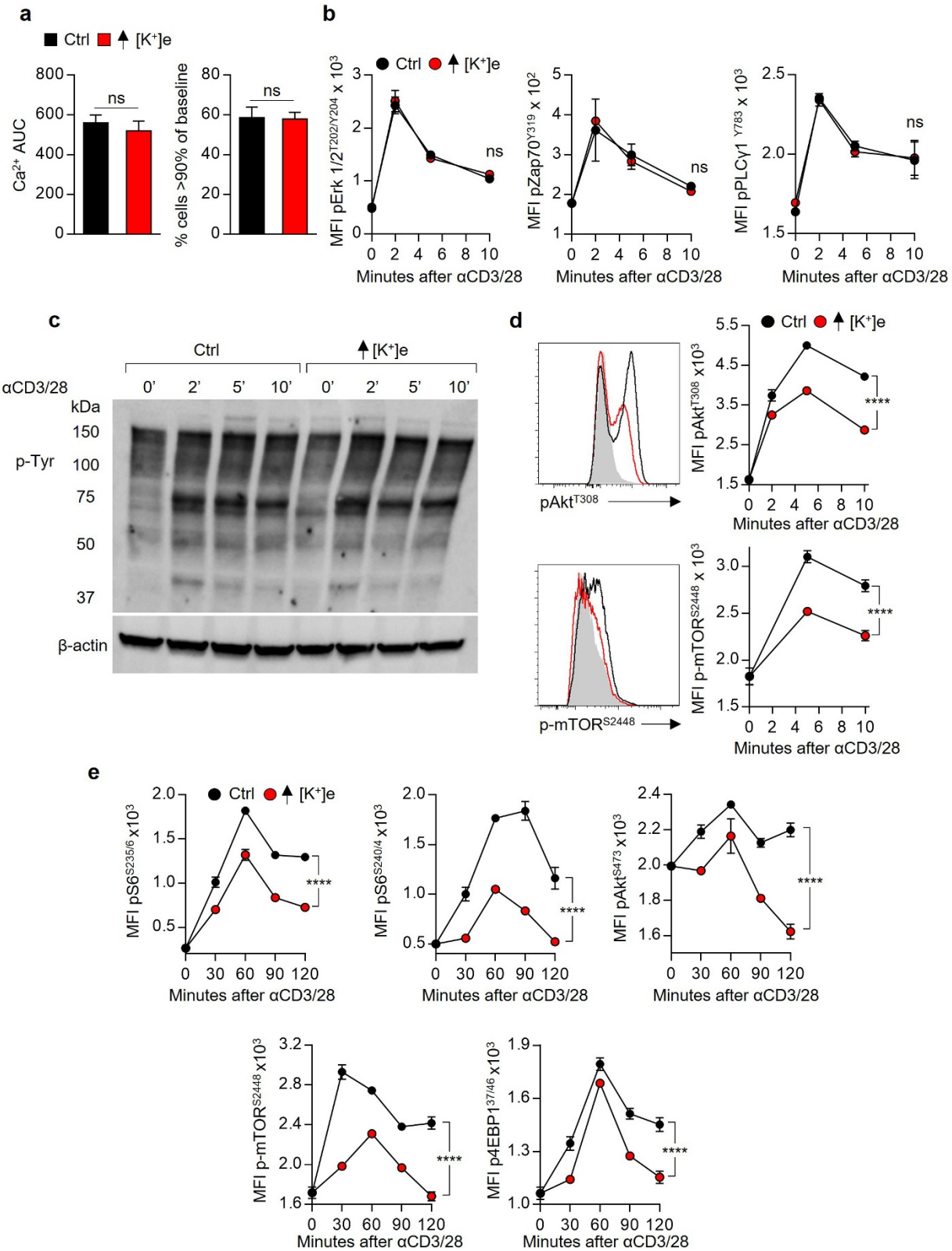

Extended Data Figure 3 | Elevated $[K^+]_e$ acts independently of TCR-induced tyrosine phosphorylation and Ca^{2+} to suppress serine/threonine phosphorylation in the Akt–mTOR axis. a, Flow cytometry analysis of TCR-induced Ca^{2+} influx in the indicated conditions (AUC, area under the curve). **b**, Flow cytometry analysis of TCR-induced phosphorylation of the indicated phospho-residues in primed $CD8^+$ T cells. **c**, Immunoblot analysis of phospho-tyrosine (4G10) residues from primed $CD8^+$ T cells stimulated as above. For immunoblot source image see Supplementary Fig. 1. **d**, Flow cytometry analysis of $CD8^+$ T cells stimulated via TCR-crosslinking for the indicated phospho-residues and representative histograms at early time points. Filled grey histograms represent unstimulated cells. **e**, Flow cytometry analysis of the indicated phospho-proteins in $CD8^+$ T cells stimulated at later time points following immobilized anti-CD3 and anti-CD28 stimulation in the indicated conditions. Elevated $[K^+]_e = 40$ mM, isotonic. Centre values and error bars represent mean ± s.e.m.; $*P < 0.05$; $**P < 0.01$; $***P < 0.001$; $****P < 0.0001$ between selected relevant comparisons. Two-tailed Student's *t*-tests (**a**, **b**), two-way ANOVA (**d**, **e**). **a**, $n = 3$ biologic replicates per condition; **b**, **d**, **e**, $n = 3$ technical replicates per data point. Representative of three (**a**–**d**) or two (**e**) independent experiments.

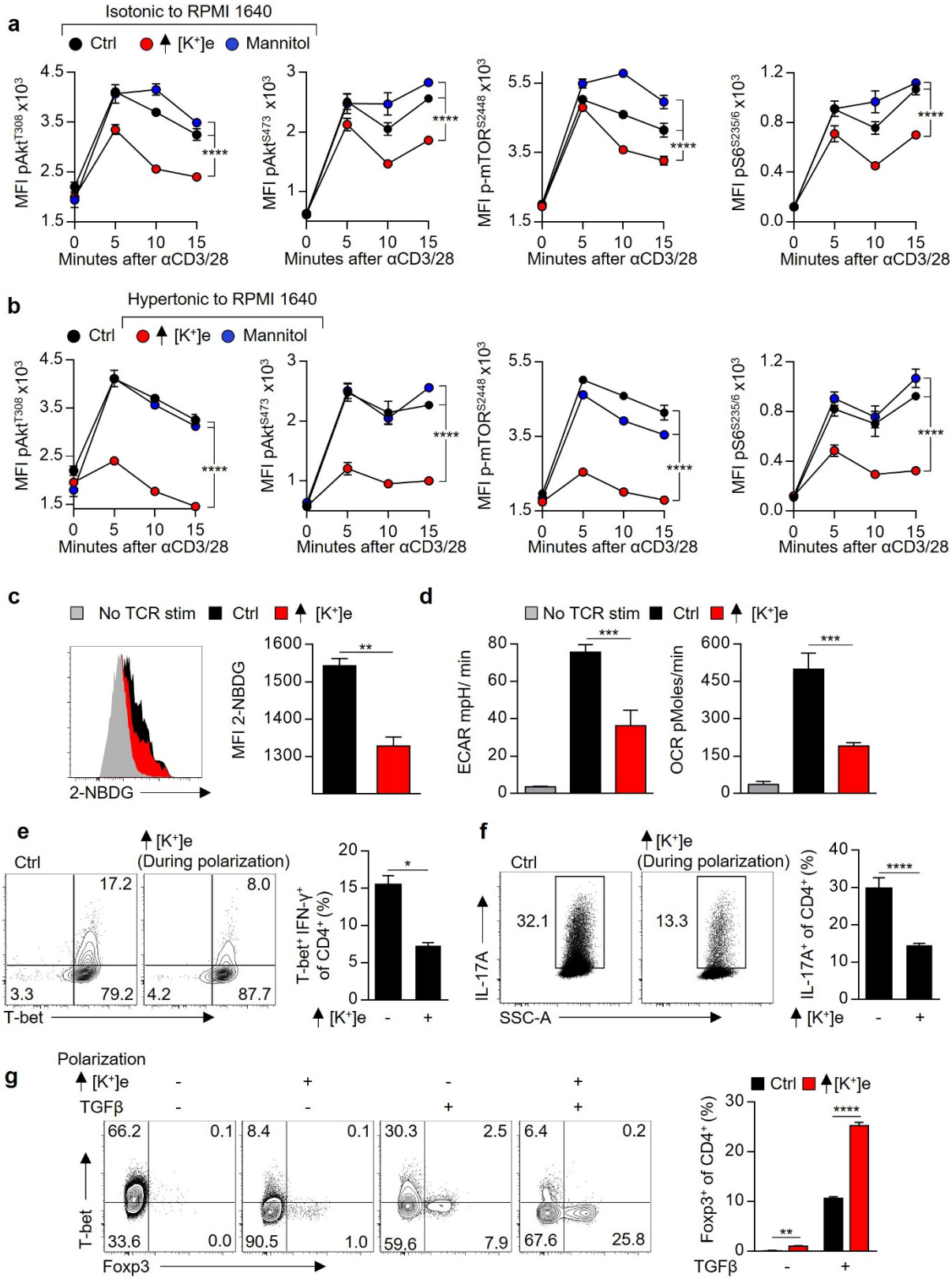

Extended Data Figure 4 | Suppression of TCR-induced Akt–mTOR signalling by elevated $[K^+]_e$ limits activation-induced nutrient consumption and T cell effector lineage commitment. a, **b**, Flow cytometry analysis of the indicated phospho-proteins in $CD8^+$ T cells stimulated by anti-CD3 and anti-CD28 cross-linking in the indicated conditions. **c**, 2-NBDG uptake in primed $CD8^+$ T cells induced by TCR stimulation in the indicated conditions with representative histograms and quantification. **d**, Seahorse XF Bioflux analysis of CD3/CD28 Dynabead-induced extracellular acidification (ECAR) and oxygen consumption rate (OCR) of $CD8^+$ T cells in the indicated conditions. **e**–**g**, Flow cytometry analysis of $CD4^+$ T cells polarized in the indicated experimental condition concurrently with T_H1 (**e**), T_H17 (**f**), or iTreg cytokines (**g**). Elevated $[K^+]_e = 40$ mM. Centre values and error bars represent mean ± s.e.m. $^*P < 0.05$; $^{**}P < 0.01$; $^{***}P < 0.001$; $^{****}P < 0.0001$ between selected relevant comparisons; two-way ANOVA (**a**, **b**), two-tailed Student's *t*-tests (**c**–**g**). $n = 3$ technical (**a**, **b**) or culture (**c**–**g**) replicates per data point. **a**–**g**, Representative of two independent experiments.

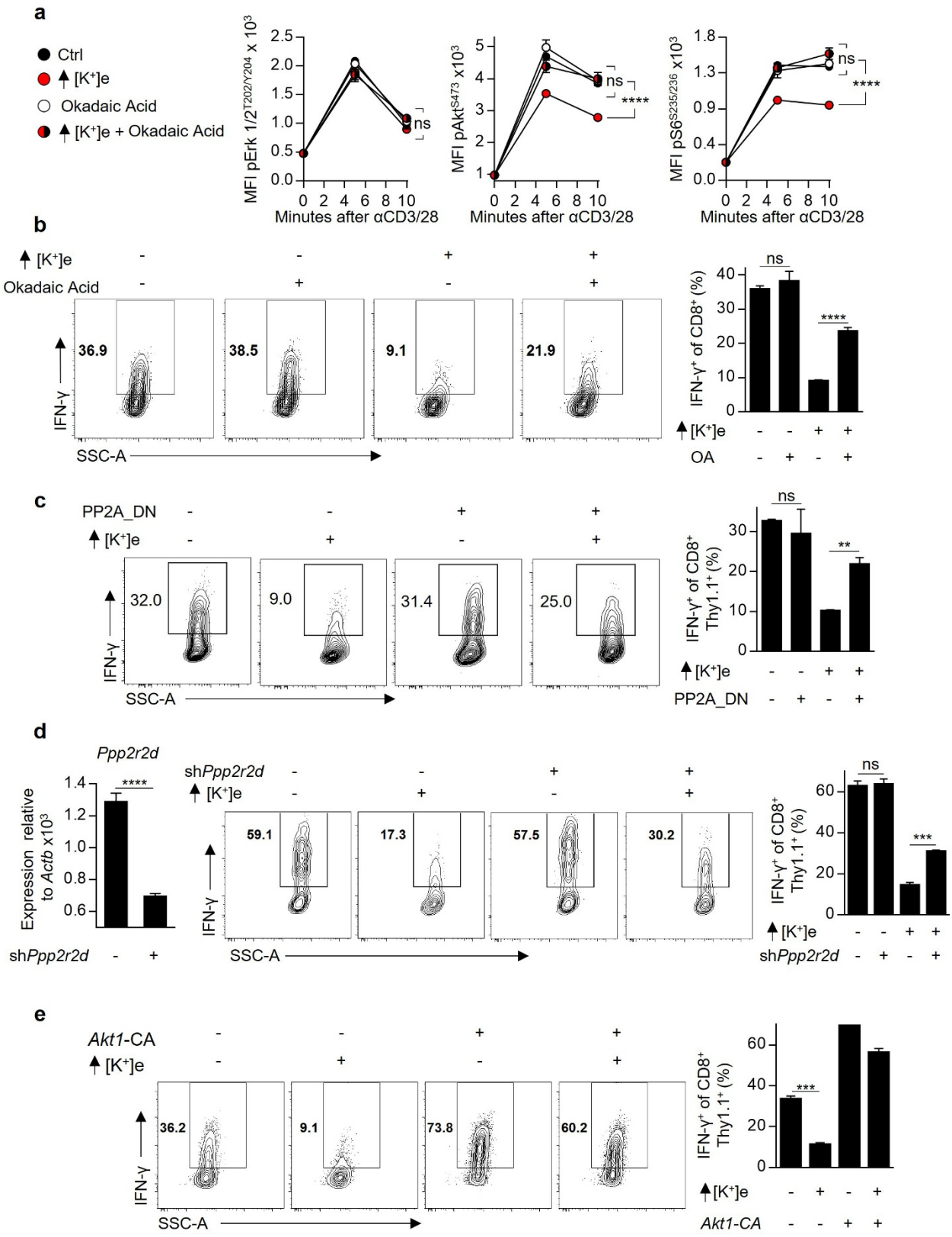

Extended Data Figure 5 | Pharmacologic inhibition and genetic disruption of PP2A function restores T cell effector function in elevated $[K^+]_e$. **a**, Flow cytometry analysis of the indicated phospho-proteins in primed CD8$^+$ T cells stimulated via TCR crosslinking in the indicated conditions. **b**, **c**, Flow cytometry analysis of CD8$^+$ T cell IFNγ production following immobilized anti-CD3/CD28 and induced stimulation in the indicated conditions (**b**), or among cells expressing a PP2A_DN isoform (**c**). **d**, *Ppp2r2d* expression in the indicated populations followed by flow cytometry analysis of IFNγ production by the populations. **e**, Flow cytometry analysis of IFNγ production by CD8$^+$ T cells expressing an *Akt1-CA* isoform stimulated in the indicated conditions. Centre values and error bars represent mean ± s.e.m. $*P < 0.05$; $**P < 0.01$; $***P < 0.001$; $****P < 0.0001$ between selected relevant comparisons. Two-way ANOVA (**a**), two-tailed Student's *t*-tests (**b**–**e**). Where noted in **a**–**e**, additional $[K^+]_e = 40$ mM. **a**–**e**, $n = 3$ culture replicates per condition and representative of at least two independent experiments.

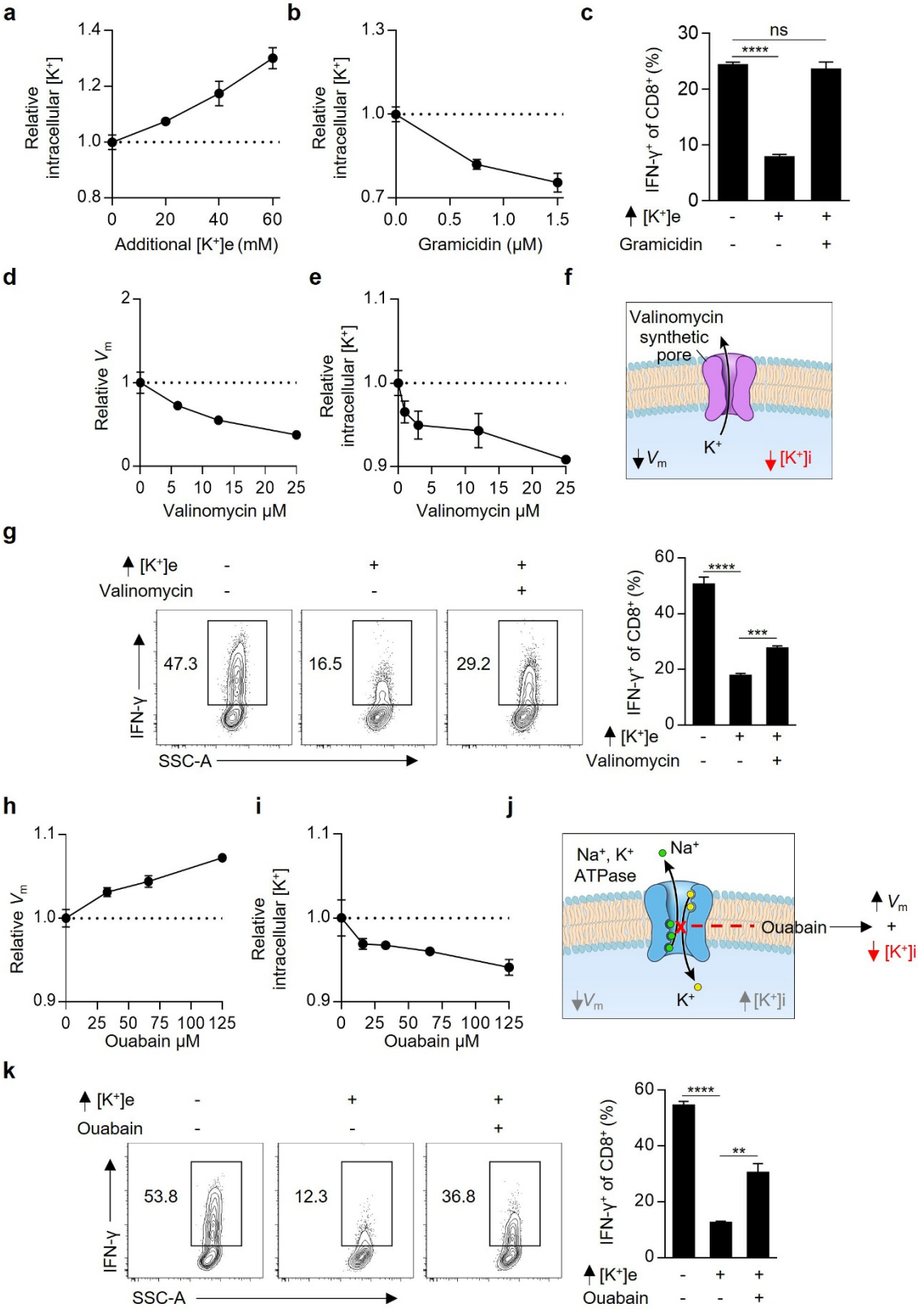

Extended Data Figure 6 | See next page for caption.

Extended Data Figure 6 | Depletion of intracellular potassium restores T cell cytokine production in the presence of elevated $[K^+]_e$. **a**, **b**, $[K^+]_i$ of $CD8^+$ T cells in the indicated conditions assayed via relative fluorescence of Asante-Green 4. **c**, Flow cytometry analysis of IFNγ production by primed $CD8^+$ T cells following immobilized anti-CD3/CD28 based activation in the indicated conditions. **d**, V_m of $CD8^+$ T cells in the indicated conditions assayed with the voltage-sensitive fluorescent indicator $DiSBAC_4$. **e**, Relative $[K^+]_i$ of $CD8^+$ T cells in the indicated conditions assayed with Asante-Green 4. **f**, Pictorial representation of the resultant intracellular changes in V_m and $[K^+]_i$ in the presence of valinomycin. **g**, Flow cytometry analysis of $CD8^+$ T cells following immobilized anti-CD3/CD28-based re-activation in the indicated conditions. **h**, V_m of $CD8^+$ T cells in the indicated conditions assayed with $DiSBAC_4(3)$. **i**, Relative $[K^+]_i$ of $CD8^+$ T cells in the indicated conditions assayed with Asante-Green 4. **j**, Pictorial representation of the resultant intracellular changes in V_m and $[K^+]_i$ in the presence of ouabain. **k**, Flow cytometry analysis of $CD8^+$ T cells following immobilized anti-CD3/CD28 based re-activation in the indicated conditions. Centre values and error bars represent mean ± s.e.m. $*P < 0.05$; $**P < 0.01$; $***P < 0.001$; $****P < 0.0001$ between selected relevant comparisons; two-tailed Student's *t*-tests (**c**, **g**, **k**). $n = 3$ technical (**a**, **b**, **d**, **e**, **h**, **i**) or culture (**c**, **g**, **k**) replicates per data point. **a**–**k**, Representative of at least two independent experiments.

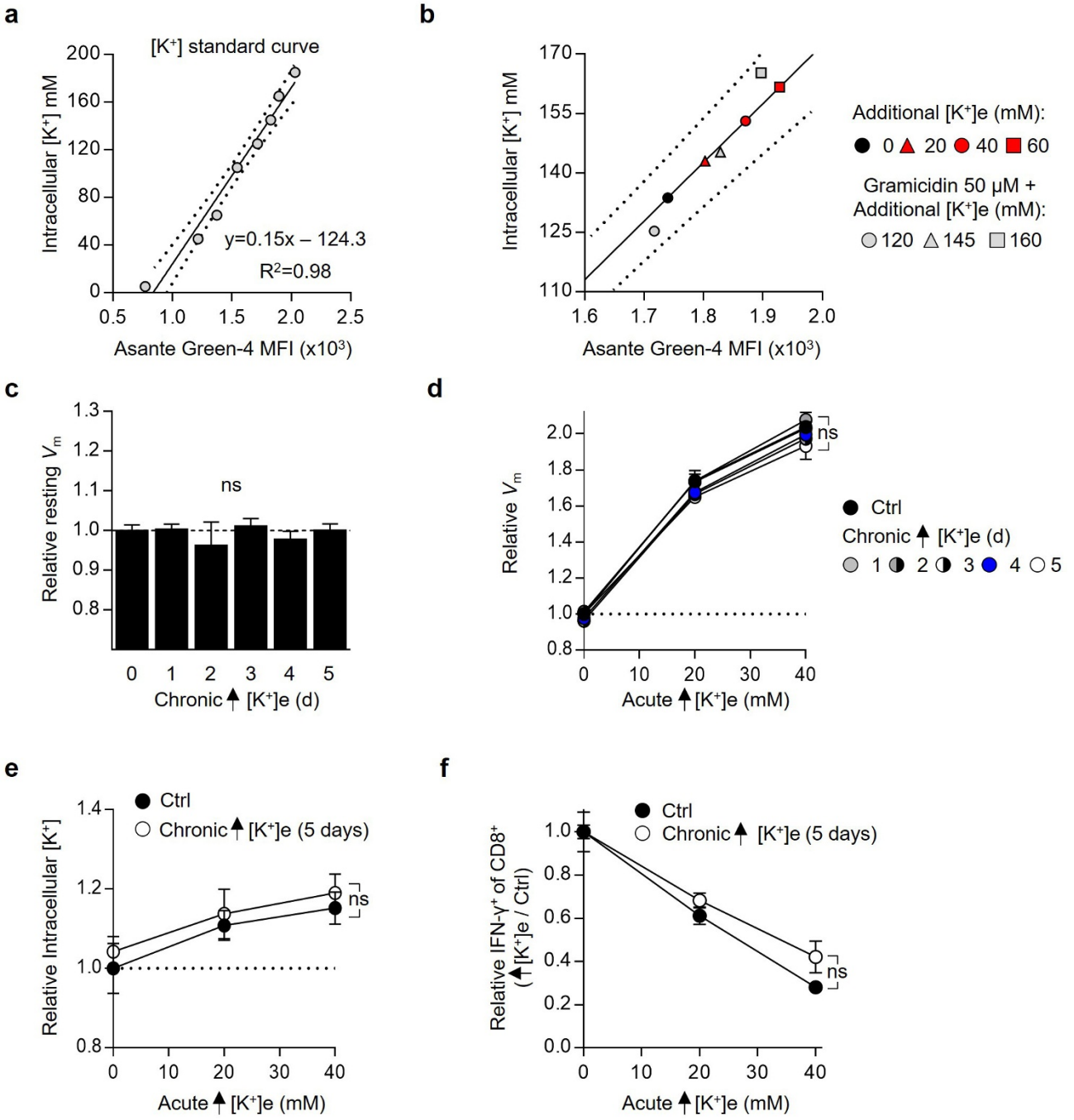

Extended Data Figure 7 | Elevated $[K^+]_e$ does not permanently affect T cell $[K^+]_i$, V_m, or subsequent response to K^+-induced suppression of effector function. **a**, Flow cytometry-based calibration of $[K^+]_i$. For all values cells were treated with 50 µM gramicidin in titrated doses of $[K^+]_e$ to provide a known $[K^+]_i$. **b**, Intra-experimental quantification of $[K^+]_i$ in control conditions and elevated $[K^+]_e$ based on calibration from **a**. **c**, Flow cytometry analysis of the relative V_m of $CD8^+$ T cells of the indicated origin using $DiSBAC_4(3)$. **d**, Cells of the indicated origin assayed in the indicated conditions as in **c**. **e**, Flow cytometry analysis of relative $[K^+]_i$ of $CD8^+$ T cells of the noted origin washed and assayed in indicated conditions, quantified by relative fluorescence of Asante-Green 4. **f**, Compiled analysis of relative IFNγ production by $CD8^+$cells of the indicated origin washed and subjected to TCR stimulation in the indicated conditions. Centre values and error bars represent mean ± s.e.m. NS, not significant, between experimental and control conditions as assessed by two-tailed Student's *t*-test (**c**) or two-way ANOVA (**d**–**f**). For chronic conditioning, additional $[K^+]_e = 40$ mM, $n = 3$ technical (**a**–**e**) or culture (**f**) replicates per condition. **a**–**f**, Representative of two independent experiments.

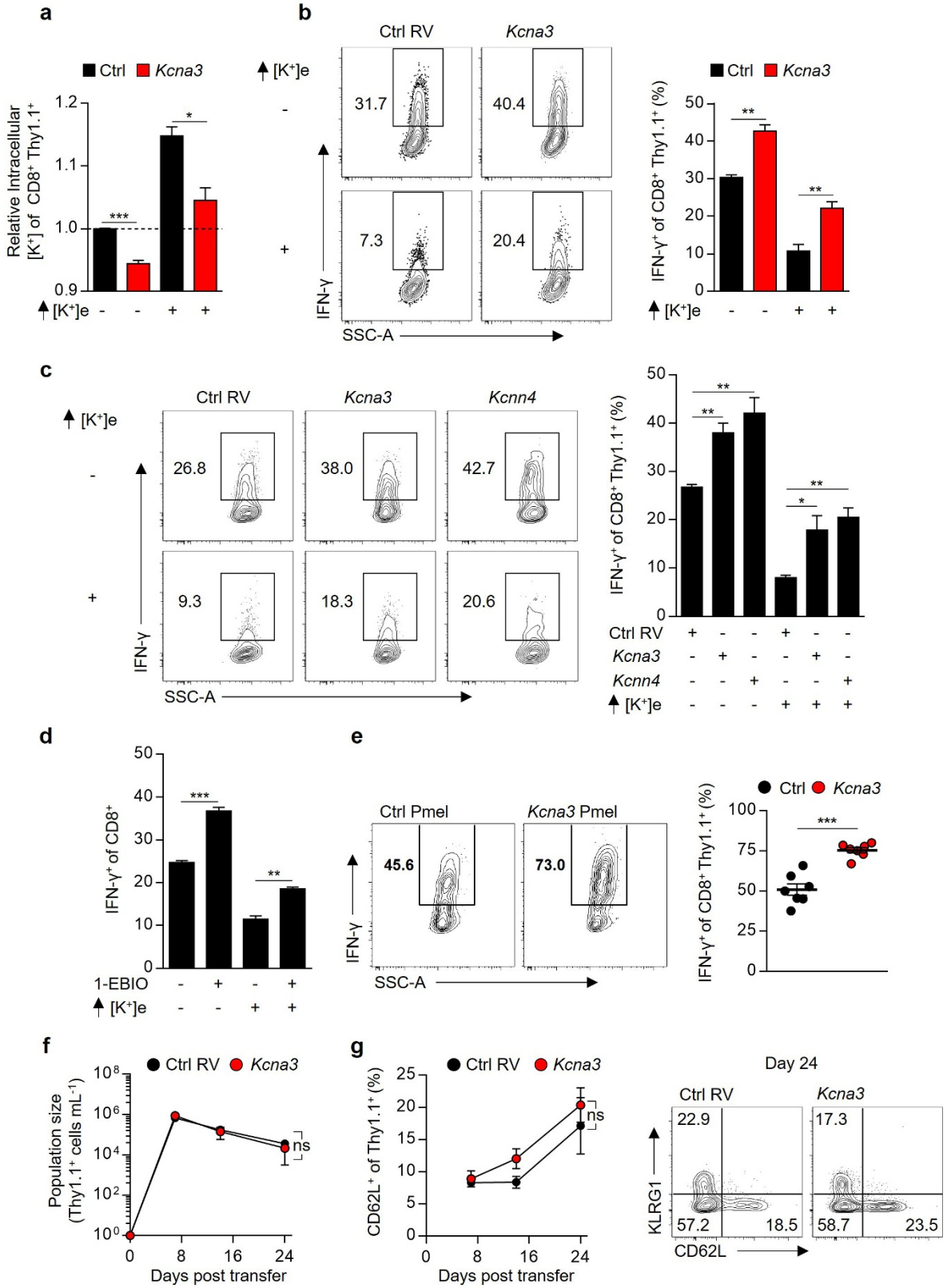

Extended Data Figure 8 | See next page for caption.

Extended Data Figure 8 | Enforced *Kcna3* or *Kcnn4* expression in CD8$^+$ T cells augments effector function. a, Flow cytometry analysis of CD8$^+$ T cells retrovirally engineered with Ctrl-Thy1.1 or *Kcna3*-Thy1.1 encoding constructs assayed for relative $[K^+]_i$ quantified by relative fluorescence of Asante-Green 4. **b**, Flow cytometry analysis of CD8$^+$ T cells following re- activation in the indicated conditions. **c**, Flow cytometry analysis of CD8$^+$ T cells retrovirally engineered with Ctrl-Thy1.1, *Kcna3*-Thy1.1, or *Kcnn4*-Thy1.1 constructs and re-activation in the indicated conditions. **d**, Flow cytometry analysis of IFNγ^+ in CD8$^+$ cells following re-activation in the indicated conditions. **e**, Flow cytometry analysis of IFNγ production in Pmel-1 CD8$^+$Thy1.1$^+$ TILs 6–8 days after transfer into tumour-bearing hosts following *ex vivo* re-activation. **f**, **g**, Pmel-1 CD8$^+$ T cells retrovirally engineered with Ctrl-Thy1.1 or *Kcna3*-Thy1.1 constructs and transferred into C57BL/6 hosts in conjunction with human $gp100_{25\text{-}33}$-encoding vaccinia virus and quantified by cell number (**f**) or surface phenotype (**g**) found in the blood of recipients. Centre values and error bars represent mean ± s.e.m.; two-tailed Student's *t*-tests (**a**–**d**), two-way ANOVA (**f**, **g**); NS, not significant; $*P < 0.05$; $**P < 0.01$; $***P < 0.001$; $****P < 0.0001$. $n = 3$ technical (**a**) or culture (**b**–**d**) replicates per condition; **e**, $n = 7$ mice per group, **f**, **g**, $n = 5$ mice per group. **a**–**g**, Representative of two independent experiments.

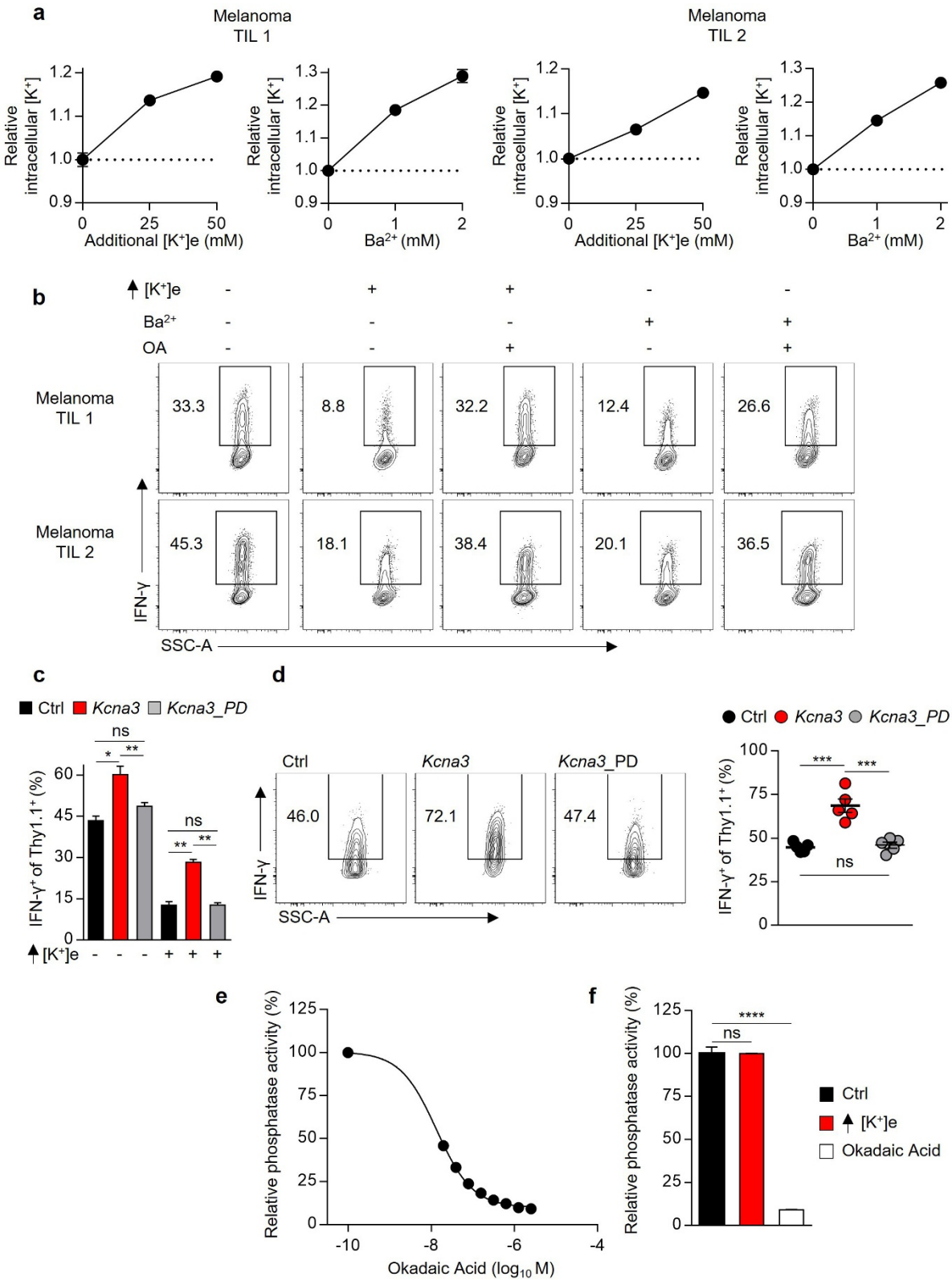

Extended Data Figure 9 | Elevated $[K^+]_i$-induced suppression of human $CD8^+$ TIL effector function requires intact PP2A activity. **a**, Flow cytometry analysis of relative $[K^+]_i$ using Asante-Green 4 on human $CD8^+$ TILs in the indicated conditions. **b**, Representative flow cytometry of the cells in **a** following TCR-based activation in the indicated conditions; quantification depicted in Fig. 4e. **c**, Flow cytometry analysis of $CD8^+$ T cells retrovirally engineered with Ctrl-Thy1.1, *Kcna3*-Thy1.1 or *Kcna3_PD*-Thy1.1 constructs. **d**, Flow cytometry analysis of $Thy1.1^+$ (transduced) Pmel-1 $CD45.1^+CD8^+$ TILs re-isolated 6 days after transfer into B16 melanoma-bearing mice and re-stimulated *ex-vivo*. **e**, **f**, Immunoprecipitated PP2A protein complexes isolated and assayed for relative phosphatase activity in titrated concentrations of okadaic acid (**e**) or the indicated conditions (**f**). Additional $[K^+]_e = 40$ mM for mouse cells and 50 mM for human cells unless otherwise indicated. Centre values and error bars represent mean ± s.e.m. NS, not significant between selected relevant comparisons; $^*P < 0.05$; $^{**}P < 0.01$; $^{***}P < 0.001$; $^{****}P < 0.0001$; two-tailed Student's *t*-tests (**c**, **f**). $n = 3$ technical (**a**, **e**, **f**) or culture (**b**, **c**) replicates per condition; **d**, $n = 5$ mice per group. **a**–**f**, Representative of two independent experiments.

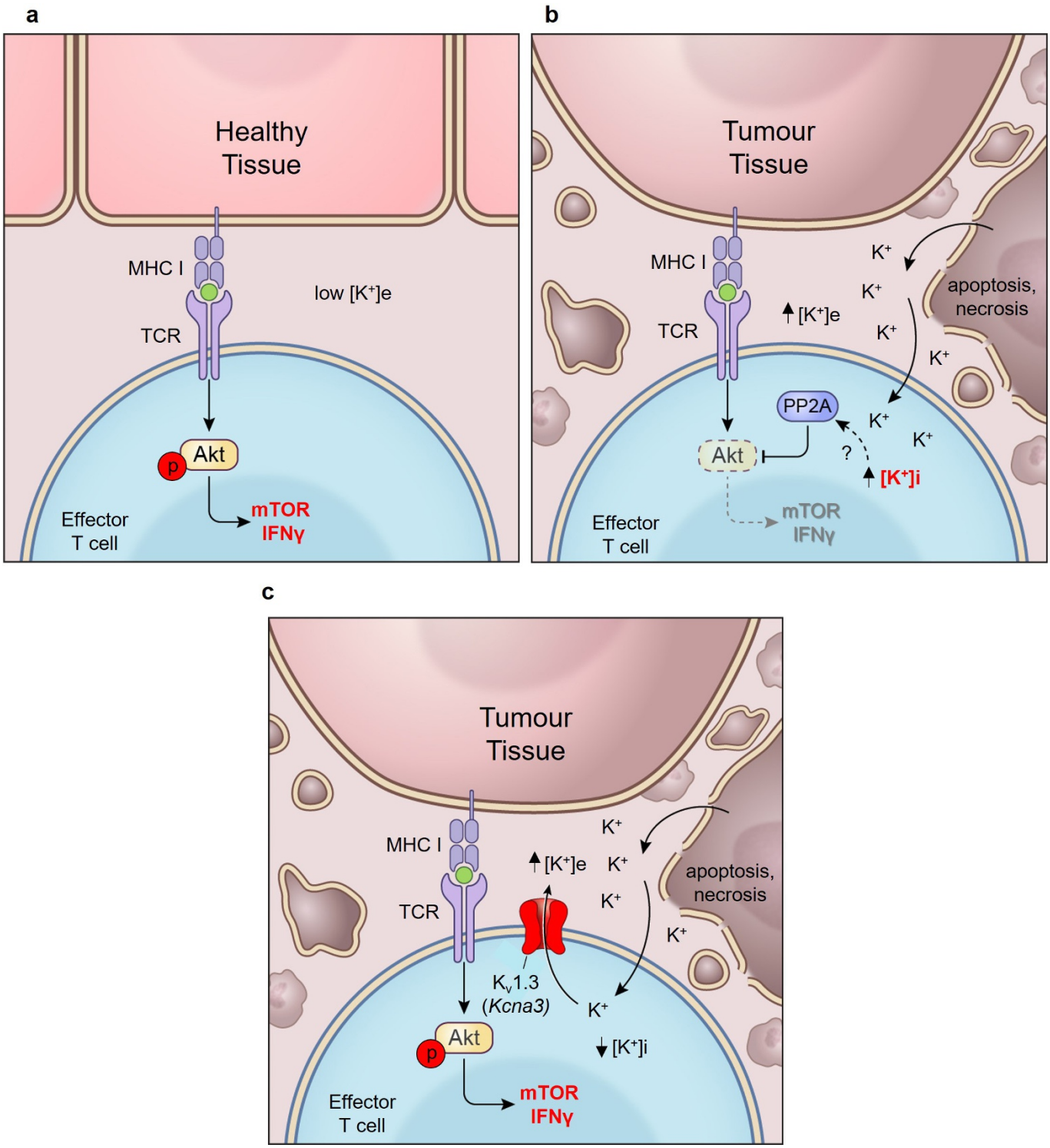

Extended Data Figure 10 | Intratumoural inhibition of T cell effector function via an ionic checkpoint. a, Healthy tissue contains limited local cellular decay, maintaining the interstitial $[K^+]_e$ close to serum levels. T cells are robustly activated following TCR stimulation. **b**, Tumour-intrinsic phenomena produce a high density of cell death within cancers. Cell death leads to release of intracellular K^+ into the extracellular space. The resultant elevated $[K^+]_e$ acts to increase the $[K^+]_i$ of T cells, limiting their activation and effector function. **c**, Reduction of $[K^+]_i$ and increased effector function can be imparted to tumour-specific T cells by overexpression of $K_v1.3$ (*Kcna3*).